TO THE GRADUATE COUNCIL:

I am submitting herewith a dissertation written by Charles Bernard Hassenboehler, Jr. entitled "FILTRATION PERFORMANCE OF CONSOLIDATED MELTBLOWN WEBS." I have examined the final copy of this dissertation for form and content and recommend that it be accepted in partial fulfillment of the requirements for the degree of Doctor of Philosophy, with a major in Human Ecology.

Larry C. Wadsworth
Major Professor

We have read this dissertation
and recommend its acceptance:

Accepted for the Council

Vice Provost and
Dean of the Graduate School

FILTRATION PERFORMANCE OF CONSOLIDATED MELTBLOWN WEBS

A Dissertation

Presented for the

Doctor of Philosophy

Degree

The University of Tennessee, Knoxville

Charles Bernard Hassenboehler, Jr.

December, 1992

Copyright © Charles B. Hassenboehler, Jr., 1992

All rights reserved

DEDICATION

This dissertation is dedicated to the memory of my parents Charlie and Katherine Hassenboehler, whose love, faith and generosity made my path easy.

ACKNOWLEDGEMENT

The author is very appreciative of the support, guidance and education provided by each of his committee members especially major professor Dr. Larry C. Wadsworth. Committee members Dr. Kermit E. Duckett, Dr. Randall R. Bresee and Dr. Wayne T. Davis provided instructive technical courses in fiber science and environmental engineering which created the academic basis for describing this work as well as help in refining this work.

Financial support from the University of Tennessee Center for Materials Processing and Exxon Chemical Company is gratefully appreciated with special note of Exxon's sponsorship of the Center.

The author recognizes with appreciation the technical expertise provided by Larry E. Spires and Richard A. Meade in processing the webs used in this research. Fellow students V. Balasubramanian, S. Kanagaraj and Ahamad Y. Khan provided broad based help in sample production, word processing, practical advice and friendship.

Finally, my wife Allie, son Chuck, daughters Khrista and Amy all provided the incentive as well as hands on help which kept the effort alive.

ABSTRACT

The purpose of this research was to investigate the effects of draw consolidation processing on the filtration performance properties of meltblown webs. Several basic parameters controlling web consolidation were examined to optimize the pore size distribution for particulate capture efficiency and other filtration performance properties. The requirements for precursor web properties and post draw processing to maximize consolidation were predicted from Euler buckling and polymer rheology principles. Variables predicted to control the magnitude of the consolidation were verified experimentally. The degree of consolidation as indicated by statistical measures of pore size distribution related collectively to the filtration performance. Webs consolidated by the draw processing achieved levels of filtration performance equivalent to webs having half the pore size.

Table of Contents

CHAPTER I 1

INTRODUCTION 1

Objectives 4

Assumptions 4

Limitations 5

CHAPTER II 6

REVIEW OF STRUCTURAL FEATURES OF FIBROUS FILTER MEDIA 6

Ordered Structures and Nonwovens 6

Filtration Efficiency 8

Meltblown Nonwovens 9

Pore Size Reduction 10

Precursor Meltblown 13

CHAPTER III 15

FILTRATION PERFORMANCE AND WEB STRUCTURE 15

Filtration Performance 15

Web Structure Consolidation 20

Filament Bonding 30

Processing Time-Temperature Effects 32

CHAPTER IV 36

EXPERIMENTAL METHODS AND MATERIALS 36

Hot Draw Processing 39

Filtration Efficiency Evaluation 40

Fiber Diameters 40

Pore Size Distribution Evaluation 40

Packing Density Measurements 43

CHAPTER V 46

RESULTS AND DISCUSSION 46

Filtration Performance 46

Time temperature effects 46

Processing Tensile Modulus 55

Bonding Level Effects 59

Air Permeability 61

Pore Size Distribution and Structural Changes 64

Steric Effects of Fiber Size 75

Conclusions 82

LIST OF REFERENCES 86

VITA 93

LIST OF FIGURES

Figure 3.1 Post draw processing illustrating lateral necking of web and strain rate inputs where V1 is the precursor web feed speed, V2 is the winder speed, and GL is the process gage length taken as the oven length. 22

Figure 3.2 Illustration of random laid filament in layer of meltblown web. . 23

Figure 3.3 Three idealized cell shapes illustrating filaments forming (left to right) a simple arbitrary shape (trivet) with a connecting filament oriented in the CD direction, a simple trivet, and the trivet having an additional filament segment bonded in the indicated MD direction. 24

Figure 3.4 Change in shape of the trivet shapes following significant MD drawing in direction of arrows. 26

Figure 3.5 Force diagram for compressive stress on transverse segment generated by tensile forces in the MD segments. 28

Figure 3.6 An isolated transverse filament segment from Figure 3.4

subjected to a critical stress to buckle filament. 31

Figure 3.7 Filament segment cell illustrating: a, rigid bonds in undrawn cell and, b, nature of shearing deformation following hot drawing in direction of arrows. 31

Figure 3.8 Plots of tensile stress as a function of modulus versus elongation of a thermoplastic polymer in three states associated with temperature levels and strain rate: a, glassy polymer state; b, leathery state; and c, the rubbery polymeric state. 33

Figure 3.9 Typical plot of log of modulus versus temperature of tensile test performed at two strain rates. 34

Figure 4.1 Meltblown pilot line at the University of Tennessee, Knoxville. . 37

Figure 4.2 Porometer (TN) flow-pressure curves for a typical sample analysis. 42

Figure 4.3 Porometer (TN) print out of a differential flow distribution for a meltblown specimen. 44

Figure 5.1 Particulate filtration capture efficiency due to hot draw post processing webs versus draw ratio for webs made at two air levels and processed at low strain rates and various oven temperatures. . 53

Figure 5.2 Particulate filtration capture efficiency due to hot draw post processing webs versus draw ratio for webs made at low air levels and processed at high strain rates and various oven temperatures. 56

Figure 5.3 Plots of tensile stress in webs during draw processing versus draw ratios at high (H), medium (M) and low (L) levels of precursor air level, and post processing temperature and strain rate. 58

Figure 5.4 Particulate capture efficiency versus post processing draw ratio for webs consolidated from precursor webs having three levels of fiber bonding: L is low, M is medium and H is a high level of bonding. 60

Figure 5.5 Plot of Fraizer air permeability versus post processing draw ratio for the consolidated webs. 62

Figure 5.6 Particulate penetration values versus air permeability data for the entire collection of samples. 63

Figure 5.7 Scanning electron photomicrographs (SEM) illustrating typical changes in the filament orientation and pore structure of the precursor web (DR = 1.0) resulting from the hot draw processing at DR = 1.75 and at DR = 2.5. 65

Figure 5.8 Porometer differential flow distribution print out for two webs: (a) a high air precursor web (DR = 1.0), and (b) the web of (a) post draw processed to a DR = 2.5. Note the large changes in the pore structure measures associated with the respective physical restructuring of filaments as shown in Figure 5.7. 66

Figure 5.9 Porometer differential flow distribution print out of a web draw consolidated to a draw ratio of 2.5 from precursor web made at the lowest melt blowing air rate. These webs experienced virtually no performance benefits from post drawing up to 150% strain. 67

Figure 5.10 Plot of maximum pore size (MAX) versus post processing draw ratio for precursor webs made at 90% die air levels. 69

Figure 5.11 Plot of maximum pore size (MAX) versus post processing draw ratio for precursor webs made at 70 and 85% die air levels. . 70

Figure 5.12. Plot of mean flow pore size (MFP) versus post processing draw ratio for precursor webs made at 80 and 90% die air levels. . 71

Figure 5.13. Plot of mean flow pore size (MFP) versus post processing draw ratio for precursor webs made at 70 and 85% die air levels. . 72

Figure 5.14. Plot of packing density versus draw ratio for webs post processed at low strain rates. 73

Figure 5.15. Plot of maximum pore size (MAX) for the collective web sample processed at draw ratio of 2.0 versus Fraizer air permeability. 74

Figure 5.16. Plot of maximum pore size (MAX) for the collective web sample processed at draw ratio of 2.0 versus particulate penetration. 76

Figure 5.17. Plot of mean flow pore size (MFP) for the collective web sample processed at draw ratio of 2.0 versus particulate penetration. 77

Figure 5.18. Plot of packing density for the collective web sample

processed at draw ratio of 2.0 versus particulate penetration. 78

Figure 5.19. Plot of the primary air level used in precursor web production versus the average diameter of the fibers in the web. . . 79

Figure 5.20. Plot of the maximum pore size (MAX) for precursor webs and counterparts post processed to DR = 2 versus the average diameter of the fibers in the web. 80

Figure 5.21. Plot of the mean flow pore size (MFP) for precursor webs and counterparts post processed to DR = 2 versus the average diameter of the fibers in the web. 81

Figure 5.22. Plot of the packing density for precursor webs and counterparts post processed to DR = 2 versus the average diameter of the fibers in the web. 83

Figure 5.23. Plot of the particulate capture efficiency for precursor webs and counterparts post processed to DR = 2 versus the average diameter of the fibers in the web. 84

CHAPTER I

INTRODUCTION

Removal of particulate from fluid streams is a problem that grows with the advancement of technologies [1]. Fabric filters for dynamic liquid and air filtration have been used to collect a broad range of particulate sizes [2,3]. Nonwoven fibrous webs offer levels of stationary microfiltration performance governed principally by the diameter of the constituent fibers. In the formation process for most random laid or unordered fibrous webs, the pore size that develops is inversely related to the square of the fiber diameter [4]. Microglass webs having fiber diameters less than one micrometer can accomplish the microfiltration demands of microelectronic clean room (HEPA) filtration, providing as high as 99.999% capture efficiency on less than 0.5 micrometer diameter particulate [5]. Typical woven and nonwoven webs having fiber diameters of several microns provide from 70 to 80 % efficiency on 5 micron particles in less demanding filtration applications such as bag house fly ash recovery [3]. Fiber fineness and the associated void fraction - one minus packing density - are fundamental parameters associated with two major aspects of filtration performance - particulate capture efficiency and pressure drop [28]. The lack of order in the deposition of fibers during nonwoven web production creates a structure which is well suited to the needs of

microfiltration. The randomness of the assembly creates a limit to the packing density which preserves permeability. This creates a distribution of pore sizes in the fibrous components of the web resulting in tortuous flow channel paths which efficiently capture particles [4].

Meltblown webs have web structural features characteristic of spunbonded nonwovens but have a broad distribution of fiber diameter sizes with the average diameter ranging an order of magnitude smaller (5 micrometers vs. 25 micrometers) than that of typical filament from spunbonded webs [6]. The micron sized fibers and the "one-shot" production nature of the meltblown process have allowed exceptional opportunities for meltblown nonwovens in the demanding area of microfiltration [7,8].

Meltblown research directed toward fiber size reduction is often motivated by the expectation of enhanced filtration performance benefits. Fiber size reduction and fiber orientation control has received attention as means toward pore size reduction in the webs [9,10,11]. Calendering webs has been applied advantageously in the development of several web products to consolidate or restructure the fibrous assembly into a thinner planar web such as calendered meltblown webs used as prefilters for membrane filters [12]. Calendering thus consolidates a web resulting in a shift in pore size distribution toward shorter and smaller flow channel pores but at the expense of reduced permeability [13]. Permeability is an important property to conserve for filtration performance.

Meltblown webs have structural assembly characteristics which allow a new approach to web consolidation. Because the filaments and constituents of the bonds (viz. filament entanglements and fused filaments) of a meltblown web are made from the same polymer, the meltblown web has a connectivity among the filaments which leads to conservation of area during a mechanical strain. Thus, meltblown web can undergo width narrowing during uniaxial drawing without destroying the planar integrity of the web. These above effects, however, have not generally been exploited because they are not recognized during tensile performance at room temperature. At elevated temperatures on the other hand, the low modulus filaments undergo gross planar restructuring during plastic deformation in which areal density is somewhat conserved.

Hardin and Keller [14] found that machine direction drawing of a particular meltblown web produced tenfold increases in the tensile strength of the post drawn web. The resultant ribbon like webs were observed to narrow in the width direction but the effect of this planar contraction on pore size control was not exploited. No prior work has addressed the concept of hot drawing precursor webs to induce pore size consolidation for enhanced filtration performance of fibrous webs. If web post drawing can be shown to alter or control the pore size distribution of the resultant web (in terms of pore size and uniformity without serious attrition of the fluid flow properties), then such webs should have enhanced particulate capture efficiencies when used as filters. The basic requirements of optimum precursor web and subsequent draw

processing should be established as a new process for filter production. This basic work is aimed at assessing the scope of hot drawing to produce webs of enhanced filtration efficiency to control pore size distribution and to identify key web and process parameters.

Objectives

The overall objectives of this research have been to address the problem of establishing the basic requirements for precursor web and post draw processing to effect optimum consolidation for enhanced filtration performance of fibrous webs. Specific objectives have been to:

1. to evaluate the extent to which web draw consolidation effects particulate filtration performance, flow properties and pore size distribution,

2. to verify the influence of initial web structural properties on the pore size distribution resulting from draw consolidation, and

3. to verify major process parameters influencing changes in web pore size distribution due to draw consolidation.

Assumptions

The following assumptions have been made:

1. basic properties of initial webs suitable for consolidation can be engineered into commercial meltblown webs,

2. web and processing concepts identified to control web pore size

distribution are valid and are applicable to meltblown webs made from thermoplastic polymers in general,

3. the post drawing apparatus used imparts no significant external compressive stress in the web to alter the thickness of the web,

4. data from all tests are valid and reproducible,

5. experimental filtration efficiency measurements from aerosol particulate penetration assesses the benefits of hot draw consolidation to modify pore size distribution of webs, and

6. establishing the principles of draw consolidation to control filtration, flow performance and pore size distribution control of meltblown webs is novel.

Limitations

The following limitations have been identified:

1. the beneficial effect of web pore size distribution alteration on barrier properties was only assessed by aerosol filtration efficiency for meltblown webs,

2. only three levels of web bonding, four levels of process air, three thicknesses, three draw temperatures, seven draw ratios, and two strain rates were evaluated for Exxon polymer grade polypropylene in the research,

3. there were a limited number of replications, and

4. consolidation of other nonwoven web types were evaluated at a minimum level to establish processing feasibility.

CHAPTER II

REVIEW OF STRUCTURAL FEATURES OF FIBROUS FILTER MEDIA

Ordered Structures and Nonwovens

Textile fabric filtration media has broad utility in particulate filtration. Separation of particulate from fluid streams is a problem that grows with advancing technology [1,5]. Fabric filters have been used to collect a broad range of particulate sizes for liquid and air filtration [15]. Typical woven fabrics having fiber diameters of many micrometers provide from 70 to 80% efficiency on 5 micrometer particles in less demanding dynamic filtration applications such as bag house systems for recovering byproducts or for pollution removal such as fly ash [3,15]. Nonwoven fibrous webs offer levels of stationary microfiltration performance that is governed by the packing density and diameter of the constituent fibers [4]. Microglass webs having fiber diameters less than one micrometer can satisfy collection required for microparticle filtration ranging down to 0.1 micrometer [1].

Woven and knitted fabrics possess structural order or a definable physical arrangement of constituents throughout their repeating physical structure. Nonwovens per se are generally fibrous webs or matts for which the fiber constituents have no spacial order or regular repeating arrangement. Some nonwovens are given post treatments such as point bonding or needling

which may or may not alter its classification as a nonwoven. In any event, the relative lack of definable order in nonwoven structures provides some notable advantages not shared with woven fabrics. On a large scale, nonwoven materials possess a distribution of web structural dimensions which can result in high void fraction or low packing density depending on the forces applied to the fibers as the nonwoven is assembled. This factor is responsible for the random size and direction of flow channels through nonwoven webs. The random size and tortuous paths of flow paths through nonwovens can provide adequate filtration efficiency on small particulate when the fluid flow rate through the web is small- a few feet per minute [16]. Because of the mezzo scale randomness of nonwoven structures, statistical methods can be applied to the structure to predict performance features such as filtration efficiency. Ordered structures made from yarns generally have bimodal pore size distributions on a macro scale associated with interyarn and interstices flow channels. The larger channels associated with interstices usually eliminate ordered fabrics from microfiltration applications. Nonwoven structures which have assembly rearrangement or defect channeling from needling or hydroentangling generally do not qualify for stationary microfiltration applications. Such post-bonding processes leave large channels analogous to the yarn interstices of ordered textile fabrics.

The pore size distribution of nonwovens is dependent on the fiber diameter and the ability of the fibrous constituents to randomly assemble under

the forces present during the particular assembly process [17]. Because of this random assembly of fibers in the construction, there is a mechanically limited or minimum packing density (one minus the void fraction) obtainable by the process. The void fraction preserves a minimal permeability. The lack of order in the assembly thus prevents closure of the voids upon consolidation. This natural process limit on solidity gives nonwovens relatively high flow per pressure drop performance compared to woven structures. In wovens, both fibers within the yarns are ordered and the yarns in the fabric are ordered.

For free formed or as-formed nonwoven structures (unconsolidated), the mean flow pore is generally related the inverse square of the fiber diameter [18]. Hence, the performance aspects of "as-formed" filtration media is fundamentally limited by the diameter of the fiber. The maximum flow pore size is often related to a multiple of the fiber diameter, i.e., 2.4 X diameter [19].

Filtration Efficiency

In the formation mechanics of random laid or unordered fibrous webs such as meltblown, the pore size that develops is related to the inverse square of the fiber diameter [18, 13]. Fiber fineness and the associated void fraction or packing density are fundamental parameters associated with capture efficiency and flow permeability -two major aspects of filtration performance [2, 20]. Microglass webs consist of sub-micrometer sized fiber diameters which translates to superior filtration performance due to pore size distribution

advantages achieved by fine fiber diameters. Stationary microfiltration for microelectronic clean rooms using High Efficiency Particulate Air (HEPA) filters provide as high as 99.999 % capture efficiency on 0.3 micrometer diameter particulate [1,5].

Meltblown Nonwovens

Like microglass, meltblown webs [21] have micron sized fiber diameters which translates to pore size distribution advantages for microfiltration. Meltblown webs are unique nonwovens that have fibrous lay-down structural features similar to spunbondeds but have a wider distribution of fiber sizes with the average fiber diameter ranging an order of magnitude smaller than that of spunbonded webs.

Some notable features of meltblown web assembly provide structural advantages for microfiltration. The filaments being added to the forming web do not typically migrate from the point of impact nor bunch together prior to or during bonding as in spunbonded webs [22]. Oncoming filaments of very low rigidity are randomly deposited and self bonded to layers of previously laid and bonded filaments. These assembly features lead to a superior narrow pore size distribution across the planar layers comprising the formed web. The micron sized fibers and the "one-shot" instant web nature of meltblown has provided meltblown technology a greater participation in the area of microfiltration.

Pore Size Reduction

In the context of this work, pore sizes is a distribution of flow channel sizes across the thickness of a web which support fluid flow. As such the individual sizes are related to the dimensions separating adjacent fibers which constitute a flow channel. A web having a general reduction in the distribution of pore sizes would require increased external pressure to expel a liquid saturating such web from the pore channels. These effective dimensions are quantified in a standardized manner by measures of incremental pressure drops required to expel immersion fluid from saturated webs according to ASTM F 316-86.

Reducing the sizes of the collection of pores in a web can be attained by (a) generating webs from fiber having smaller diameter which are fitted together more closely, or (b), by densifying webs of fixed fiber size or fiber size distribution to externally increase the packing density of the web. Research efforts toward uniform and finer fiber size distributions in webs [7,9,11] provide a direct path to the reduced pore size distributions required for extended microfiltration applications for meltblown. Ongoing developments in meltblown resins, die and collector hardware, and processing technology have improved fiber size and web uniformity and low basis weight capabilities [8, 10, 12, 13]. Present capability to commercially produce fine fiber web at controlled packing densities for use in high level microfiltration is limited [8].

While as-formed meltblown webs characteristically have superior flow-

pressure drop performance, pore size reduction methods to physically consolidate the structure greatly reduce the permeability of webs as solidity increases. Calendering to densify or press the fibrous assembly into a thinner planar web or product has been applied advantageously in the development of several web innovations. The commercial fabric SMS of The Kimberly Clark Corporation, is an example of a point bonded laminate in which the meltblown center layer - the functional barrier fabric - undergoes limited and favorable planar compression between the outer spunbonded layers which is maintained by the point bonds across the face area of the fabric [23]. Consolidating the fibrous elements in the thickness direction often flattens fibers and closes flow channels thus decreasing the relative flow properties of the web media.

Enhanced machine direction fiber orientation aerodynamically induced during meltblowing using an oscillating device is claimed to create an oriented filter structure without calendering [24]. A review of prior work on consolidation by means other than calendering has revealed drawing processes to create uniformity in films, rovings and webs [14,25,26]. Biaxial drawing of polymer films is aimed at increasing strength and structural uniformity.

Extensive uniaxial drawing of fibrous webs and films [25] has been used to produce high strength ribbons based on improved molecular orientation. A narrow polymer web or film is drawn while in contact with a series of dovetailing heated transverse bars to create ribbons of high strength. No indications are made regarding the effect of this processing on changes in the pore size

distribution of the ribbon product.

In the Harding and Keller [14] patent, particular meltblown webs having a low degree of molecular crystallinity and orientation were post drawn in an oven to produce strong ribbons having a ten fold increase in strength and high luster. Although the webs consolidated or narrowed in width in the post drawing process, only strength and luster enhancement were evaluated. No mention of pore size alteration was given. Scanning electron micrographs (SEM's) in the patent comparing the face pore structure of the special precursor web and the post-drawn web product reveal uncertain changes in the size of the maximum pores seen through the plane of the web.

Uniaxial drawing of fibrous webs from textile grade fibers is not expected to create significant lateral consolidation suitable for controlling pore size distributions. A minimum level of lay down randomness of the laid thermoplastic filament and bonding integrity under drawing conditions is required for a web to experience significant lateral contraction with uniaxial drawing - a Poisson effect. Precursor webs having fiber to fiber thermal bonding or filament entanglement in a randomized web are good candidates for pore reduction effects during uniaxial post drawing. Ericson [27] utilized orientation effects to overcome the tendency of spunbonded carpet fabrics to narrow during stretching by increasing the number of filaments oriented in the machine direction. This strategy altered the room temperature biaxial stress-strain behavior of the carpet by increasing the MD tensile stiffness.

In bonded fibrous webs from processes using either (a) fibers having high tensile properties evident by high molecular orientation or low elongation at drawing temperatures, or (b) bonding means which degrade or fail in holding power at post draw processing temperatures, or (c), low levels of filament entanglement bonding, the bonding can fail during draw processing and diminish the stresses on the filaments that contribute to transverse narrowing of the web pores. For example, some carded or air-laid webs of textile grade fiber which are bonded by a low melting temperature bonding fiber content would exhibit minimum transverse contraction with drafting or other hot draw processing. In webs such as air or wet laid webs, interfiber bond forces are either negligible or too stiff to overcome and pore size distribution changes are insignificant.

Precursor Meltblown

Precursor webs used in the Harding and Keller process have specific features which allow extensive drawing. The effects of the draw process were independent of temperature. Filaments in the initial web are highly bonded and are quickly quenched to minimize crystallization of the PP and can sustain draw ratios up to 10 to 1. The polymer is degraded to a specified level and web structure is developed to simulate tensile performance properties analogous to undrawn filament for the precursor web..

Because the very entangled filaments and interfiber bonds of their

meltblown web are approximately a continuum of the same low modulus polymer, the web sustains high levels of uniaxial draw processing without rupturing. No prior work has addressed the concept of establishing precursor and post draw process strategies designed to maximize pore size consolidation for enhanced filtration performance of webs. The manner and extent to which web pore size distributions can be altered and controlled by hot drawing has not been approached from the standpoint of developing draw consolidation processing for enhanced filtration performance of meltblown. This is the aim of this work.

CHAPTER III

FILTRATION PERFORMANCE AND WEB STRUCTURE

The considerations below are intended to identify web structural factors that influence particulate filtration performance of fibrous webs, and to predict precursor web properties and post draw processing requirements to effect pore structural alteration for enhanced filtration.

Filtration Performance

The random deposition of micrometer size fiber or filaments in a nonwoven web creates small scale structural uniformity that lends itself to statistical prediction of pressure drop and filtration efficiency. The lack of order and lack of periodic faults makes nonwoven webs well suited to the demands of microfiltration. High stationary capture efficiencies at relatively high air velocities without the benefit of cake development makes up the challenge in microfiltration.

Two critical properties relative to filtration performance are capture efficiency and flow permeability or pressure drop. Particulate capture efficiency can be expressed in terms of the number of particles which traverse a filter as follows,

$$\eta = (Ni - Np) / Ni$$

where Ni is the number of particles challenging the filter and Np is the number

of particles penetrating the filter. This expression can be reduced to

$$\eta = 1 - (Np/Ni)$$

and by defining Np/Ni as the dimensionless penetration P, the expression becomes

$$P = 1 - \eta$$

Numerous researchers have developed equations to predict aspects of filtration performance for filters of various porosities and flow regimes. Fuchs paper in Orr [28] was the first to calculate aerosol particulate collection of high packing density (low porosity) fibrous webs. He attributed overall collection to individual capture efficiency mechanisms due to diffusion, interception, gravitational, and inertial impaction. Inspection of how the separate collection mechanisms are affected by structural parameters of the web will indicate strategy for altering web structure to enhance filtration performance.

In a recent paper, Liu and Rubow [4] summarized equations utilized to predict filtration performance for fibrous webs. They assembled the pertinent equations and achieved excellent predictions for pressure drop and airborne particulate capture efficiency for a range of intermediate porosity nonwoven webs using the single fiber efficiency approach to prediction [28]. In their treatment, individual fiber efficiency coefficients for particulate capture by diffusion and interception were isolated as dominating mechanisms of capture for the application. Their resultant single fiber efficiency ηs represented by the summed collection coefficients is given by

$$\eta_s = \eta_d + \eta_r$$

Then, an overall collection efficiency for airborne particulate is given by

$$\eta_l = 1 - \exp(-\eta_s \times S)$$

where S is defined as a filter area factor for the specific filter equivalent to the axial cross sectional area of the entire length of fiber - single fiber - in the web and given by

$$S = \text{frontal area of fiber in web}$$

$$S = 4 \times \text{basis weight}/ \pi D_f \rho_f.$$

Thus, the overall efficiency increases with the surface area of the web, and surface area for a web of given basis weight increases with decreasing filament diameter D_f and fiber density ρ_f for fiber constituents having circular cross sections.

Lee and Rubow used specific coefficients from Liu and Lee [29,30] to described the individual theoretical single fiber efficiency terms. Diffusion is defined to occur when small particles passing close to an element of the collector (e.g., a fiber in the web) diffuses toward the fiber and is subsequently held at the surface by a variety of other forces such as van der Waals or electrostatic. The single fiber term for diffusion was

$$\eta_D = 2.58 ((1-c)/k)^{1/3} Pe^{-1/3}$$

where c is the packing density given by the quotient of the basis weight by the product of the web thickness and the fiber density. The Peclet number (Pe) is a dimensionless number and its reciprocal characterizes the intensity of

diffusion deposition expressed as

$$\eta_D \ \alpha \ Pe^{-1} = D / U D_f$$

where D is the diffusion coefficient for the particulate in a particular air mass.

Capture by interception (designated by subscript R) is defined to occur when a particle's center of mass misses a collector element, but, because of its finite size, the particle strikes the object or element [3]. The theoretical single fiber efficiency for interception capture given in Lee and Liu [30] is

$$\eta_R = ((1 - c)/K) (R^2/(1 + R))$$

where R is an interception parameter representing the ratio of the size of the depositing particles D_p to the fiber diameter D_f and given by D_p/D_f. Thus, the coefficient for single fiber collection by interception is characterized by

$$\eta_R = (D_p/D_f)'2 / (1 + D_p/D_f) = dP'2 / (D_f'2 + D_pD_f)$$

Both ηD and ηR are seen to increase as web structural parameters of c and the inverse D_f increase.

Polypropylene meltblown webs made with lower packing densities are sometimes given permanent electrostatic charging and used as high efficiency filters known as electrets. Electrets can be utilized at higher face velocities U with low pressure drops. In such webs, coulombic attraction and inertial impaction can become the dominate contributions to the expression for single fiber efficiency. The coulombic charges on filaments or particles alters collection efficiency by influencing the particle trajectories by electric field forces and the particle adherence to fiber surfaces by attraction of opposite charges

[28]. The coulombic single fiber collection efficiency component is typified by

$$\eta_C = Q \cdot q / (D_p D_f U).$$

Again ηc has structural dependence of the inverse of D_f. The D_f term is the diameter of the particle.

The single fiber collection coefficient due to inertial impaction is greatly involved with the parameters of the velocity field about the collector fibers and the inertia of the particles. Inertial impaction deposition is defined to occur when the center of mass of the particle collides with an element of the collector. Collection by this mechanism increases with particle size and flow velocity. The basic concept for inertial impaction collection is that of a target striking efficiency [28] characterized by the ratio of an inertial stopping distance Xs for the particle to the diameter of the fiber collector D_f.

Thus, from the above, the general observation is made that structural packing density and fiber diameter have a consistent influence on the various collection coefficients relating to overall filtration efficiency. Fiber collection efficiency increases with increased packing density and inverse fiber diameter.

Theoretical equations for Darcy's Law regime pressure drop dP and fluid flow at face velocity Vg across filter made from randomly deposited filaments of diameter D_f in a flat web follow a form given by Davies [31] as shown below,

$$dP = 16\ c\ u\ Vg\ h / Ku\ D_f^2.$$

This equation generally holds for such filters at low gas velocities and low Reynolds numbers such as those experienced in HEPA filters [4]. Ku is the

hydrodynamic factor related to structural flow channels and is proportional to the resistance of flow through the cells or channels formed by the deposited filaments. Kuwabara's hydrodynamic factor Ku used by Liu and Rubow is a function of the packing density c of the web given by

$$Ku = - 1/2 \ln c - 3/4 + c - c^2/4.$$

As the packing density and inverse fiber diameter increase, the pressure drop increases and the face velocity decreases. For any family of like webs, a particular empirical correction is required to compensate for theoretical overprediction of values which applies universally to pressure drop, permeability and collection efficiency. Correction factors are attributed to velocity field prediction errors due to inhomogeneity of structure, errors in measuring packing density, and nonperpendicular flow over fiber segments [32]. Meltblown and other spunbonded webs in the class of spunbondeds are relatively homogeneous structures within the plane filaments compared to needled or hydroentangled webs.

Thus altering physical structure of fibrous webs, such as increasing the packing density and reducing the filament diameter, enhances the overall particulate collection efficiency based on the single fiber collection considerations above but at the expense of reduced flow or increased pressure drop.

Web Structure Consolidation

The packing density and average fiber diameter attained from melt

blowing or other formation processes are limited by the energy intensity of the web forming process and the viscosity and other properties of the polymer. For some spunbonded webs, the filaments have molecular orientation and possess good tensile properties and have a very narrow distribution of diameters. Filaments in a typical meltblown web vary widely in diameter and the birefringence and tensile modulus of individual filaments increases with decreased filament diameters attained. Meltblowns possess levels of filament bonding, inter filament entanglement and extensibility of filaments which promote lateral contraction when the web is uniaxially drawn at elevated temperatures. Microscopic examination of such laterally consolidated meltblown web specimens indicated a potential for post drawing to control packing density - a factor in collection efficiency.

In hot draw processing, as schematically illustrated in Figure 3.1, a precursor web 1 is fed into an oven at speed V1 and withdrawn at speed V2 and the web structure is consolidated laterally via geometric alteration of the web filaments. Consider the schematically depicted microscopic assembly of randomly deposited and variously attached (bonded or entangled) filaments forming a thin planar layer of a meltblown web, as represented in Figure 3.2. While the random planar disposition of the fiber in meltblown webs is not reducible to a unit cell per se, representative cell shapes of academic utility are illustrated via the solid straight line segments depicted in Figure 3.3. When the

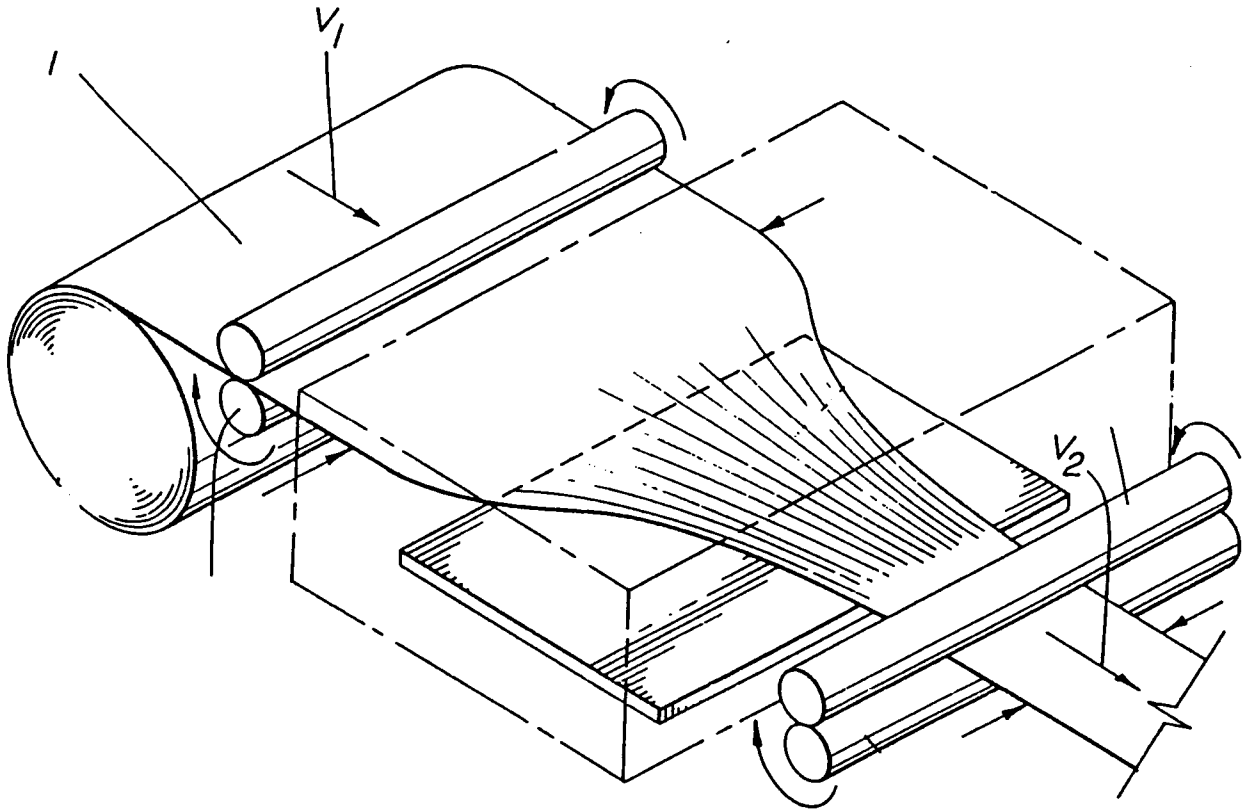


Figure 3.1 Post draw processing illustrating lateral necking of web and strain rate inputs where V1 is the precursor web feed speed, V2 is the winder speed, and GL is the process gage length taken as the oven length.

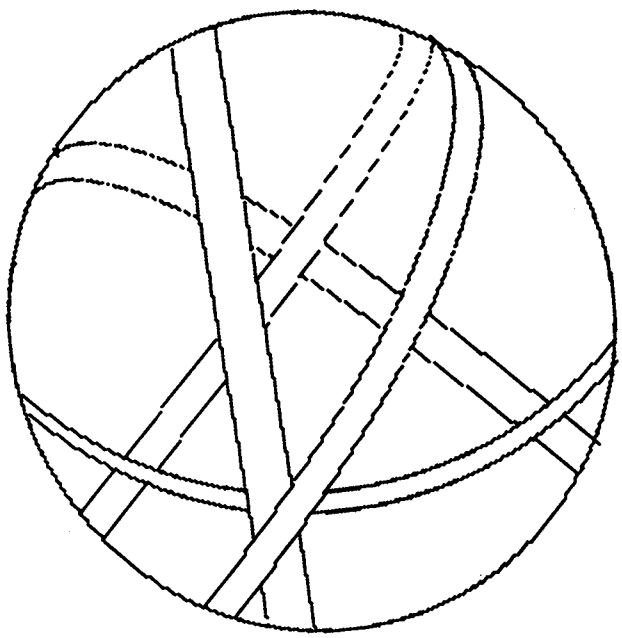


Figure 3.2 Illustration of random laid filament in layer of meltblown web.

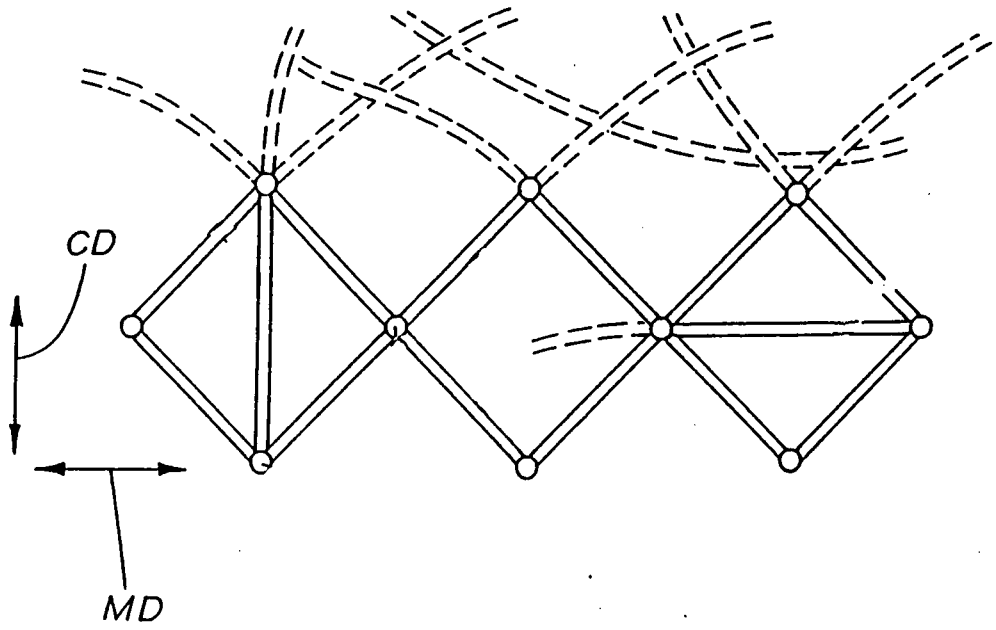


Figure 3.3 Three idealized cell shapes illustrating filaments forming (left to right) a simple arbitrary shape (trivet) with a connecting filament oriented in the CD direction, a simple trivet, and the trivet having an additional filament segment bonded in the indicated MD direction.

idealized assembly of fiber in Figure 3.3 is subjected to a strain in the machine direction (MD), segments of filaments generally oriented toward the machine direction (e.g., segments oriented in the MD + - 45 degrees) undergo tensioning while filament segments generally oriented transversely (i.e., the cross direction + - 45 degrees) are subjected to compressive stress which impose buckling forces on the transverse segments. When uniaxial drawing is imposed on thermoplastic material above the softening temperature of the filaments, the array of thermoplastic segments can deform plastically as shown in Figure 3.4 depending on the physical properties, bonding, and dimensions of the fibrous elements.

An estimate of the minimum level of draw required to close the various microscopic cells of a randomized web can be attained by considering the assembly in Figure 3.3 as an idealized assembly of pin connected stiff elements having no buckling resistance. The collection of all cells have an average initial orientation of 45 degrees to the direction of MD uniaxial drawing. Then by the Pythagorean Theorem, the web draw ratio required to close trivet shaped cells as indicated by (a) in Figure 3.4 is the square root of 2 or a draw ratio of 1.41. Thus, theoretically a machine direction strain of 41% is required to maximize the structural consolidation via uniaxial draw processing.

In the process of uniaxially post-drawing webs at polymer softening temperatures, filament segments in the CD direction are buckled away from or our of the cross direction depending on the magnitude of the compressive

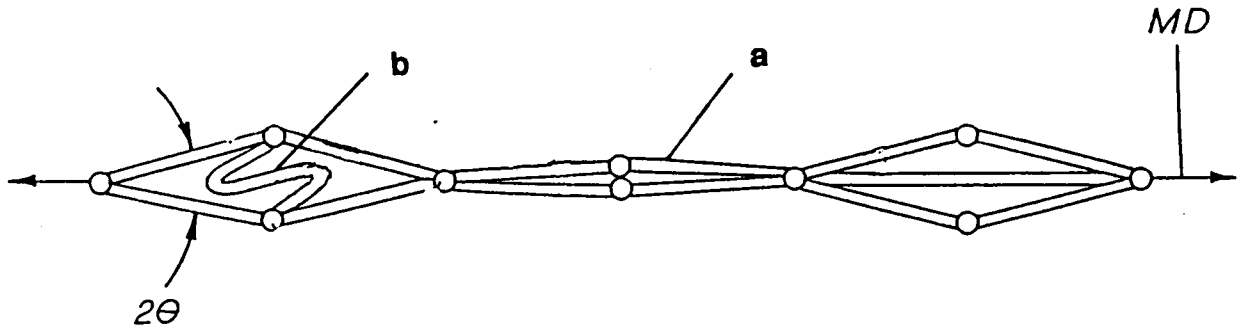


Figure 3.4 Change in shape of the trivet shapes following significant MD drawing in direction of arrows.

load and buckling resistance as indicated by (b) in Figure 3.4. Being plastically deformed and heat set during the hot drawing process, the buckled segments persist as finite spacers limiting the lateral compaction or separation between adjacent elongated MD filaments. The change in diameter of the filament segments due to the draw elongation is assumed to be negligible at the low draw ratios observed.

The compressive stresses on filament segments generally oriented in the CD are generated by the tension developed in the MD elements due to MD processing draw or elongation as illustrated in Figure 3.5. By triangulation, the resultant compressive stress sigma)c on a transverse filament segment is

$$\sigma_c = 2\ T \sin \theta$$

where θ is the angle between the filament segment and the MD direction and T is the tension which is a function of the temperature related tensile modulus, the strain, and the diameter of the filament. The compressive stress and thus structural consolidation is maximized for larger tension T and large angle θ.

The relationship between structural buckling and tensile stresses on the bound filament system can be approximated using Euler's Buckling equation. In isolation, the critical compressive stress σ_c to induce buckling is described in Figure 3.6. The critical stress effectively increases with the filament modulus E and the square of the fiber radius r as indicated below

$$\sigma_c = \pi\ E\ /\ (L/r)^2 = \pi\ E\ D_f^2\ /\ (4\ L^2)$$

where L is the buckling beam length. The quantity L/r is the slenderness ratio

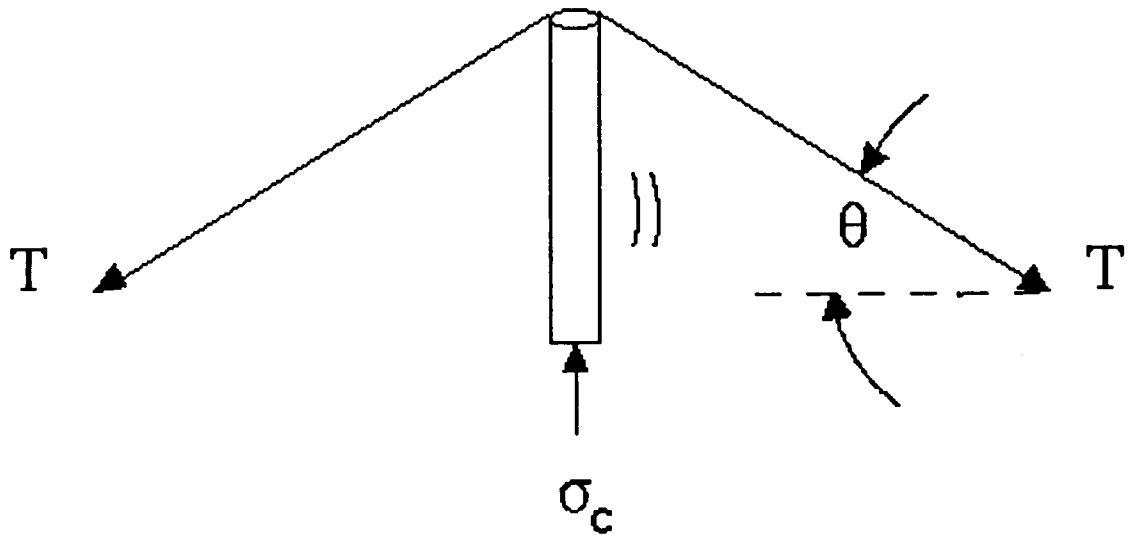


Figure 3.5 Force diagram for compressive stress on transverse segment generated by tensile forces in the MD segments.

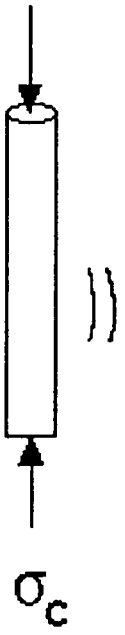


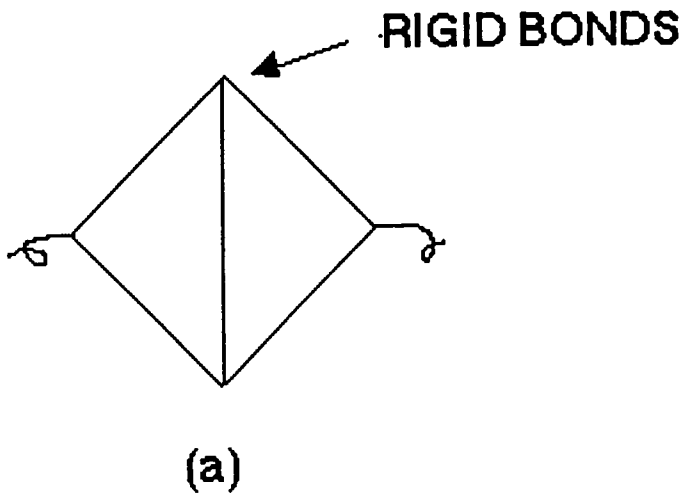
Figure 3.6 An isolated transverse filament segment from Figure 3.4 subjected to a critical stress to buckle filament.

of the filament. If the bonded system is considered as a unit as in Figure 3.3, then trial and error solutions are required to resolve the tangent modulus solution to the critical buckling stress [33]. When considered in isolation as in Figure 3.6, buckling and thus consolidation is maximized when the modulus E and the length to radius slenderness ratio of the filament segment under compression are decreased.

Filament Bonding

In addition to fiber diameter, modulus, and buckling effects, the strength and rigidity of interfiber bonding imposes a limit to CD consolidation effected by drawing. Weak interfiber bonding with significant filament entanglements is analogous to a pinned bar (fiber) engineering system and would permit minimum resistance to lateral consolidation. Interfiber entanglements among the randomly laid elements would insure lateral contraction.

Rigid fiber-to-fiber bonds which occur in some meltblown webs are expected to have an overall negative effect on web consolidation. Such fusion bonding of filament segments as schematically shown at a in Figure 3.7 for an unstrained web illustrates the effect of compressing bars with fixed ends [33]. Rigid bonds inhibit easy deformation as filaments must undergo shear deformations that create the effect of short buckling lengths L as indicated in the highly elongated cell of rigid bonds at b in Figure 3.7. Thus increased fusion bonding between filaments in the precursor web should limit lateral



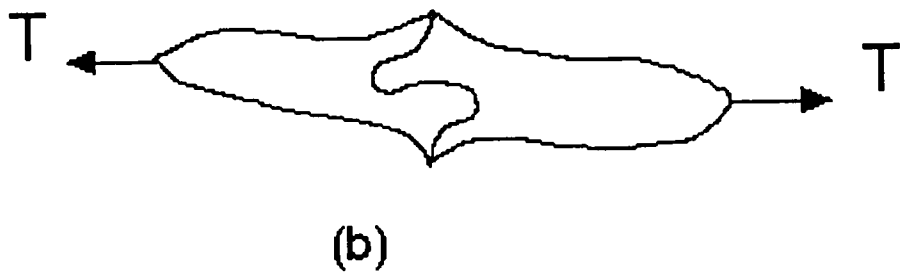


Figure 3.7 Filament segment cell illustrating: a, rigid bonds of undrawn cell and, b, nature of shearing deformation following hot drawing in direction of arrows.

planar consolidation by post draw processing.

Processing Time-Temperature Effects

During the post drawing process, the effective modulus while the filament segments are being drawn depends on process time-temperature effects. Figure 3.8 shows the deformation stress versus temperature relationship for a typical thermoplastic polymer processed at three rheological states: a, glassy polymer state; b, leathery state; and c, rubbery state. The modulus of the polymeric material is given by the initial slope of the curve. The typical dependence of the modulus and tensile stress of a viscoelastic polymer on the rate at which the strain is imparted, i.e., strain rate, is illustrated in Figure 3.9. A twenty fold increase in relative processing time at higher temperatures increases the modulus by one order of magnitude. In post draw processing, the strain rate ε is given by the difference between web takeup speed V2 and web feed speed V1, divided by the gage length GL over which the transition in web dimension occurs, as illustrated in Figure 3.1 and the equation that follows.

$$\varepsilon = (V2 - V1) / GL$$

Thus in the hot draw process, decreasing the web processing temperature and increasing the processing strain rate maximizes the filament modulus and tension during the consolidation process to achieve maximize lateral plastic deformation. This creates maximum tensions at greater angles to produce higher compression on CD oriented filament segments. Maximum

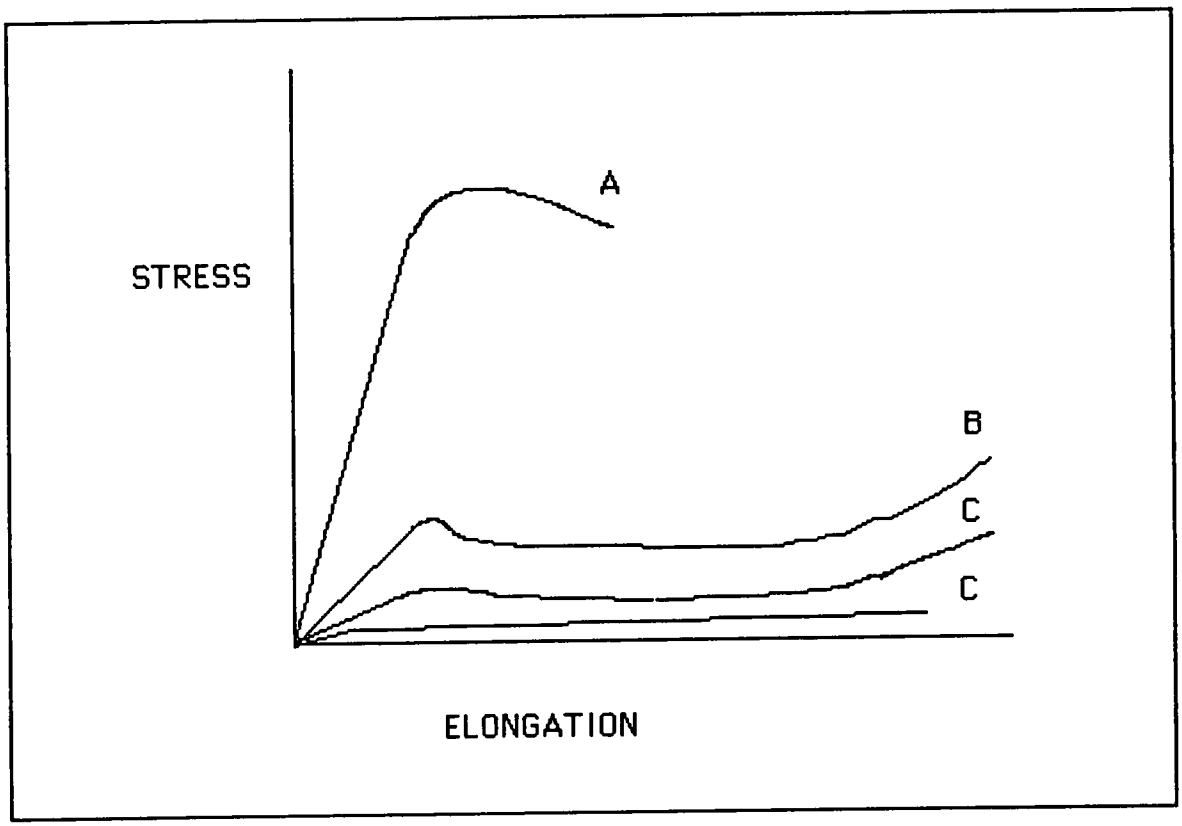


Figure 3.8 Plots of tensile stress as a function of modulus versus elongation of a thermoplastic polymer in three states associated with temperature levels and strain rate: a, glassy polymer state; b, leathery state; and c, the rubbery polymeric state.

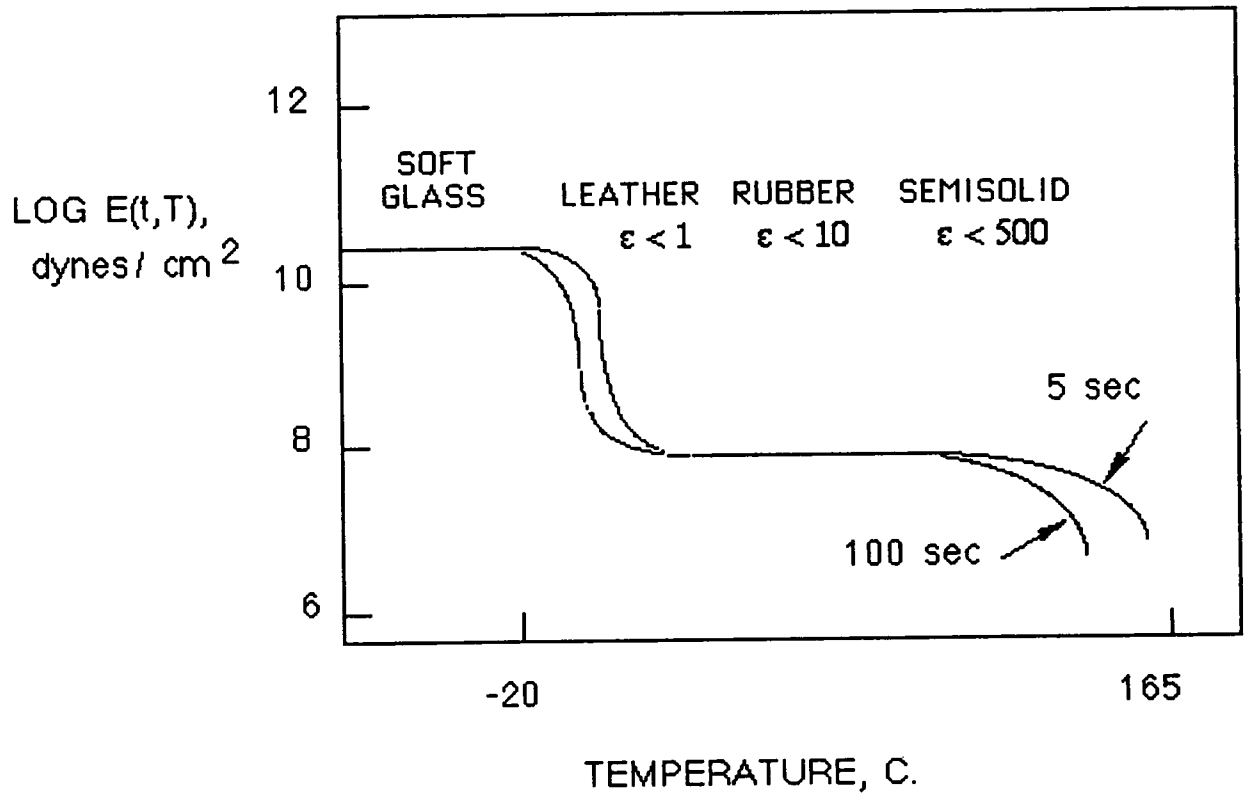


Figure 3.9 Typical plot of log of modulus versus temperature of tensile test performed at two strain rates.

consolidation is achieved at a trial and error modulus at which the compressive stresses overcome, to the largest extent, the critical buckling stresses for the CD segments in the web.

CHAPTER IV

Experimental Methods and Materials

All meltblown samples evaluated in this research were made using a 20 inch line at the University of Tennessee. The line is schematically shown in the Figure 4.1. Sets of meltblown web samples were made for which the effects of precursor web and post processing variables on filtration performance measures could be evaluated. Filtration performance was based on aerosol particulate capture efficiency and air permeability. Basic effects of bonding level, fiber diameter, web tensile modulus during draw, processing draw ratio, and other time-temperature effects on the filtration performance of the webs were determined.

Various sets of precursor webs were made at processing air levels of 70, 80, 85 and 90 % of the full open position of the air supply valve and combinations of other web formation variables in order to evaluate the above. With other die related parameters held constant, the air valve opening was used to control the average filament diameter of the webs. The degree of molecular orientation developed or present in the filaments due to the formation process is related to the birefringence of the filaments. Moreover, the tensile modulus and the maximum elongation attained during drawing (i.e., hot drawability) is linked to the diameter and molecular orientation of the filament in the web [7, 34, 35].

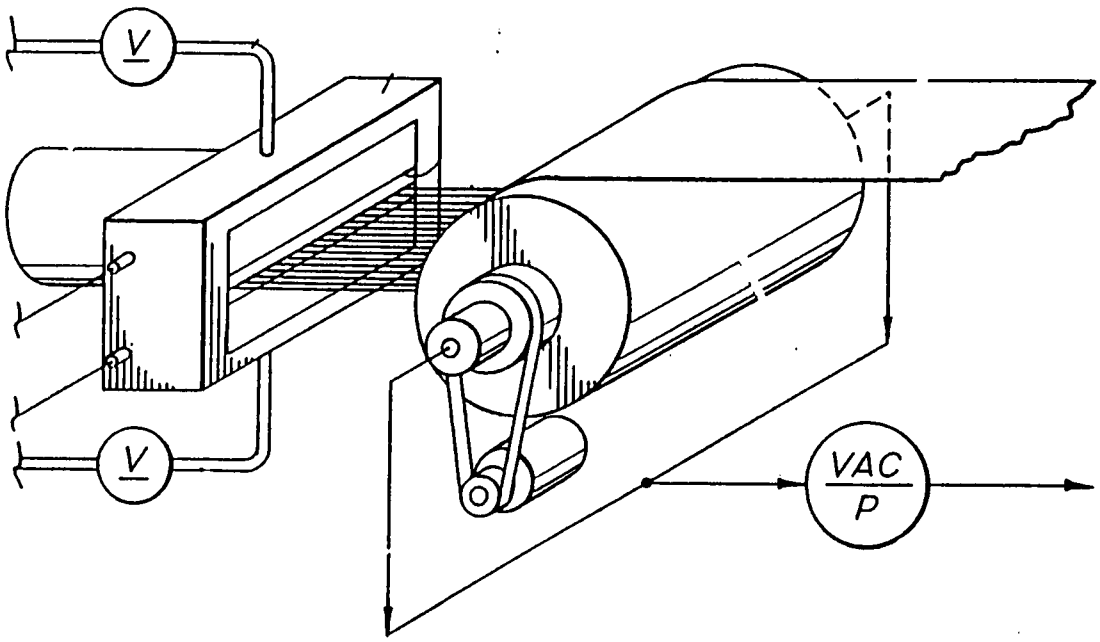


Figure 4.1 Meltblown pilot line at the University of Tennessee, Knoxville.

Precursor webs having high and low levels of tensile drawability corresponding to 90% and 80% air levels, respectively, were made to evaluate time-temperature and draw level effects of post processing. Samples from each set were processed at seven levels of draw ratio to 2.50 and two levels of strain rate up to 4000 per minute (units are reciprocal minutes).

The level of bonding in meltblown webs effects the tensile properties such as strength and elongation at break. Two sets of precursor webs were made at 85% and 70% air valve setting. Webs in each set were given three levels of bonding between filaments identified as high, medium and low bonding. Elongation at break was utilized to quantify the bonding strength or level for the six samples. The bond strength for the precursor was increased by increasing the flow of hot air flowing through the web as it formed on the collector surface by controlling the level of vacuum inside the collector. The relationship between web breaking elongation ε_B and the rotation rate (RPM) of the vacuum pump drawing jet air into the collector surface of the meltblown line was linear and was given by

$$\varepsilon_B = C\ (RPM) - 500$$

where C is a constant for this specific set of webs and RPM is pump rotor rotation rate in revolutions per minute. Levels of bonding produced at RPM values of 500, 1000 and 1500 were rated as low, medium, and high bonding for each of the two sample sets.

Hot Draw Processing

Preliminary post draw processing was done on various meltblown and other specimens using an Elna (TM) brand clothing ironing press apparatus to estimate ranges of samples, draw ratio, temperature, and other variables to evaluate. The experimental precursor sample set made for further evaluation in this work were made on one of the twenty inch lines at the University of Tennessee. The post draw processing was done on an experimental apparatus comprising a web unwind or feed roll, heating oven and takeup roll as shown schematically in Figure 3.1.

A padding mandrel was extensively modified to provide a speed controlled, web feed roll, rolls for directing the web into the oven, and web take out roll driven by a variable speed or variable torque DC drive motor. Tensile stress developed in the web during continuous steady state processing at each draw ratio was measured using a three roll tensionometer. A top loading digital balance having a low friction roller fixed to the pan of the balance was used as the load measuring roll of this tensionometer. The drawing tension T on the web during processing was computed from the load F recorded by the balance and the angle θ subtended by the web passing over the three roller system. The tension was a function of the sine of the angle θ and the normal force F due to the tension in the web given as $T = F / 2 \sin \theta$.

Filtration Efficiency Evaluation

Particulate capture efficiency tests using nominal 1.0 μM monodisperse dry latex particles at an aerosol flow of 10 cm/s as described in ASTM 1989 - 15, were performed to evaluate the filtration performance of the experimental specimens. Pressure drops across the specimens were recorded for the 10 cm/s air flow across the specimens. Computations of the overall filtration efficiency according to Benjamin Liu theory equations (ASTM STP 975/1986) were done using a Basic computer program. The efficiencies were computed for the above test parameters of 1.0 μM particles and 10 cm/sec face velocity.

Fiber Diameters

Data to compute average fiber diameters of precursor webs were obtained from direct measurements of fiber diameters from SEM photographs of the specimens. Approximately one hundred fibers per sample were measured for computation of the average fiber diameters reported.

Pore Size Distribution Evaluation

A Coulter Porometer (TN) instrument was used to obtain measures of pore size distribution of the set of pores in the experimental webs following ASTM F 316 - 86. The method employs a special case of the Washburn Equation for capillary rise for which the contact angle for the Porofil (TN) wetting agent and the web is unity. In the pore size distribution analysis

operation mode, the Porometer machine initially increases the air pressure on the wetted sample in incremental steps and thus expels the wetting fluid from the largest pores firstly and finally expels the wetting liquid from the smallest pore channels of the subject web. Each event in which the rate of air flow exceeds the expected flow for the instantaneous pressure drop is linked to an incremental addition in flow through newly opened pores in the specimen. Thus, each measured flow event is associated with a specific pore size computed using the instantaneous pressure data via the Washburn relationship:

$$\text{Pore Diameter } (\mu M) = 40\,\gamma\,(mN/m) / P\,(mbar)$$

where γ is the surface tension of the Porofil wetting liquid saturating the web structure having units mN/M and P is the pressure in mbar.

Following complete removal of the wetting fluid by the increasing air pressure on the specimen, a second air flow - pressure drop run is performed on the now dry specimen. From subtracted differences between the flow-pressure curves for the wet and dry runs, various distributions of the data are created to describe the measures of pore size distribution of the web. Figure 4.2 shows an idealized flow-pressure curve from a Porometer instrument run depicting the origin of three fundamental data points of interest in pore size analysis determinations. The bubble point or maximum pore size (MAX) is specified as the pore size associated with the flow event in which the first amount of liquid is expelled from a subset of pore channel sizes which are the largest in the web specimen. This subset may contain one or more pores of

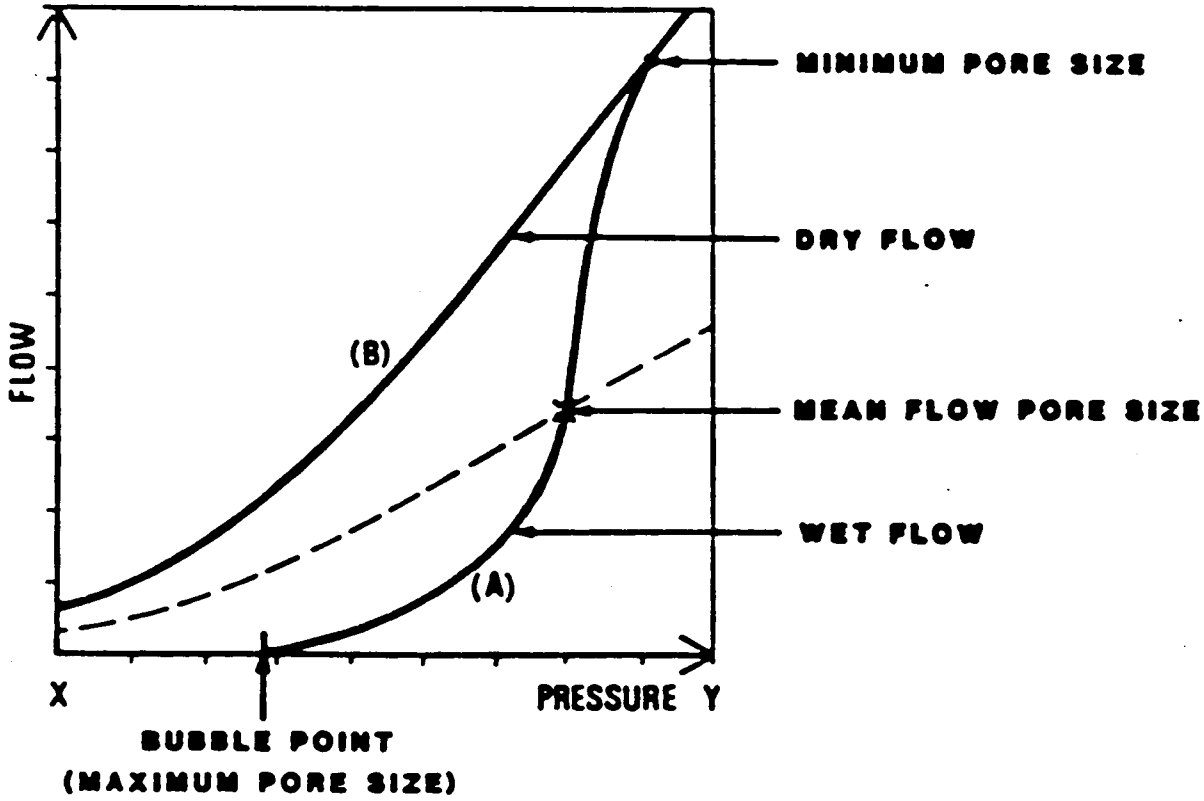


Figure 4.2 Porometer (TN) flow-pressure curves for a typical sample analysis.

this maximum size. MAX marks the onset of flow as pressure is increasing on the initially saturated specimen. The absolute dimension of this MAX pore sizeis determined from the event-pressure drop and the above pore diameter equation by the Porometer software. The minimum pore size (MIN) is computed from the pressure value associated with the point at which the wet flow curve (marked A in Figure 4.2) and the subsequent dry flow curve (marked B) intersect. At this point, liquid has been expelled from the smallest of pores. A mean flow pore size (MFP) is computed using the pressure associated with the point of intersection between a line bisecting the dry run flow-pressure curve with the wet flow curve shown as the dashed curve in Figure 4.2. The slope of the flow pressure drop curve is indicative of the permeability of the particular web.

Various flow and number distributions of pores versus pore diameter are computed from incremental volumetric flow increases. A particular distribution of interest is the differential flow distribution as shown in Figure 4.3. Each point on the curve is a measure of the differential flow, in percent of the total flow, associated with the pore size related to the pressure at the point. A vertical dotted line marks the MAX or bubble point. The MIN and MFP and MAX are displayed at the inset legend of the Porometer print out in Figure 4.3.

Packing Density Measurements

The packing density (c) of the web is a measure of bulk density and is

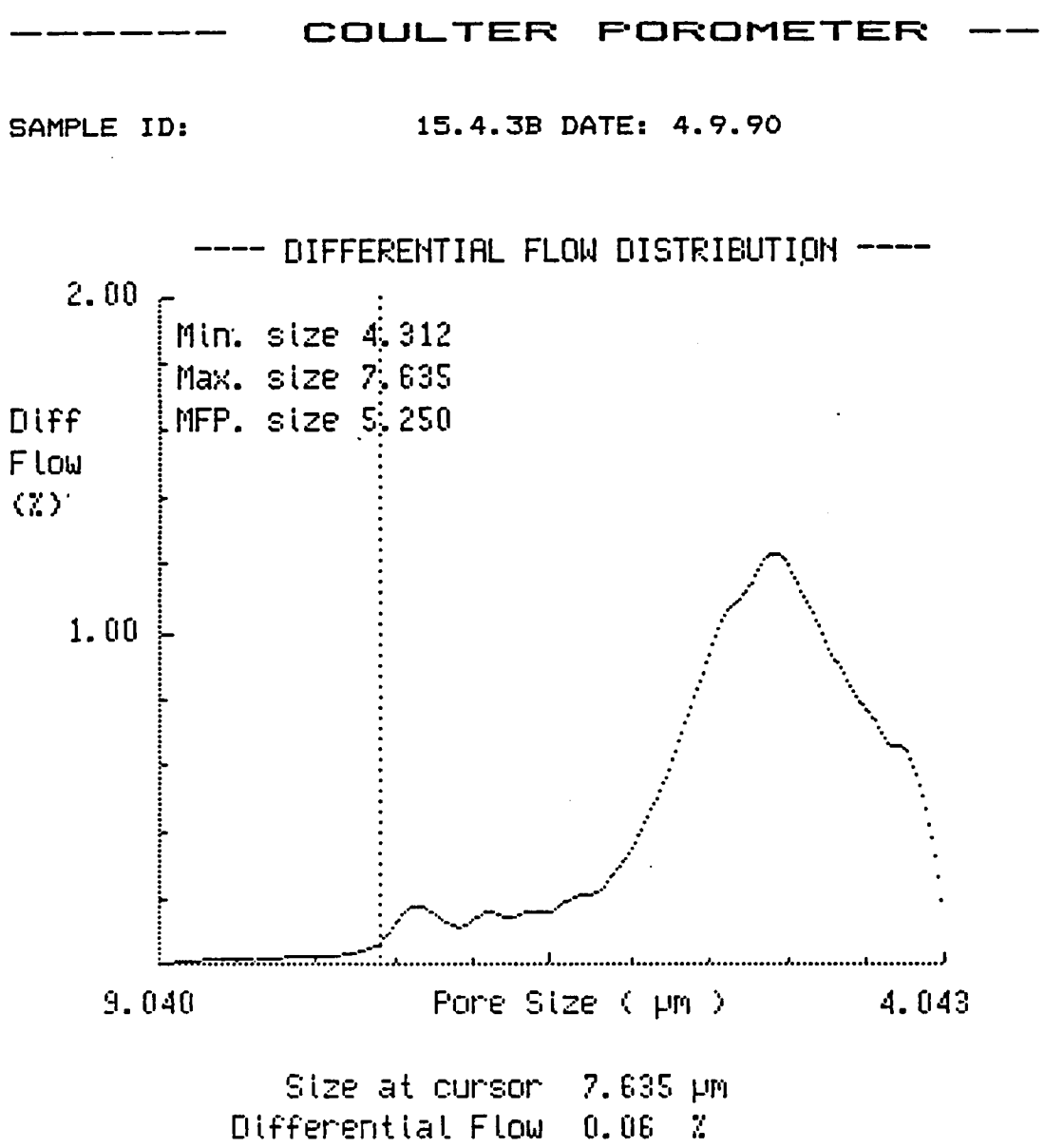


Figure 4.3 Porometer (TN) print out of a differential flow distribution for a meltblown specimen.

equivalent to one (unity) minus the porosity of the web. Packing densities were determined by a liquid immersion method based on the assumption that a measurable mass of liquid of known density fills the void space within the space bordering the fibers making up the web. The packing density c is expressed in terms of the ratio of the mass of the fiber in the space to the mass of solid polymer filling the space bordering the web can be written as

$$c = DW / (DW + VV * \rho_f)$$

where DW the dry weight is the weight of the dry web and ρ_f is the density of the filament polymer. The void volume VV within the space bordering the web is

$$VV = (WW - DW) / \rho_L$$

where WW the wetted weight is the weight of the liquid immersed web and ρ_L is the density of the liquid. By substitution, the packing density reduces to the following

$$c = 1 / (1 + (WW / DW) (\rho_f / \rho_L) - (\rho_f / \rho_L).$$

The liquid used was 1-Propanol and the filament polymer was polypropylene.

CHAPTER V

Results and Discussion

Filtration Performance

Results of hot draw processing and precursor web variables on the measured filtration performance of consolidated webs are recorded in Table I and Table II. The results will be discussed and interpreted relative to measures of particulate capture efficiency, flow and pressure drop performance and measures of pore size distribution for the altered structure of the processed webs.

Time temperature effects

The effect of time-temperature processing [35] parameters were evaluated on precursor webs made at 90 and 80 air valve settings. These precursor webs could be characterized as having soft and harsh handle relating to high and low air level, respectively. Subsequent processing differences were in strain rates, oven temperatures, and draw ratios as indicated in the specimen description in the materials section of chapter 4.

The process feed rate V1 for the precursor web entering the oven was fixed and the variation in web removal speed V2 created a range of strain rates thereby allowing time-temperature effects to be investigated. Figure 5.1 illustrates the particulate capture efficiency effected in the precursor webs due

Table I . Processing and performance data for consolidated webs.

Sample Number	Draw Ratio	Fil Effic %	Press In.Wa.	Fraizer CFM	MAX μM	MFP μM	MIN μM	Packing Density
1.0	1.00	16.3	0.02	110	35.0	18.0	14.0	0.132
1.2	1.50	22.8	0.02	132				
1.3	1.75			72				
1.4	2.00	40.6	0.18	54	21.3	11.6	9.5	0.199
1.5	2.25	33.9	0.18	71	16.2	12.6	9.3	0.217
2.0	1.00	20.0	0.02	141	35.6	22.0	13.8	0.196
2.2	1.5	43.6	0.18	53				0.176
2.3	1.75			33				
2.4	2.00	55.3	0.42	24				0.227
2.5	2.25			20				
2.6	2.50	60.9	0.58	20	11.4	8.8	6.5	0.247
2.7	2.75			19	10.3	7.7	5.2	
2.8	3.00	58.7	0.52	22				0.25
3.0	1.00	27.1	0.08	93	26.1	20.7	12.5	0.101
3.2	1.50			51				0.121
3.3	1.75			30				
3.4	2.00	69.0	0.58	19	12.9	8.8	6.0	0.197
3.5	2.25			22				
3.6	2.50			16	11.5	7.9	4.5	
3.7	2.75			18	9.8	7.5	5.0	
4.1	1.00	46.1	0.08	81	31.0	14.7	11.6	0.087
4.2	1.50	68.6	0.46	19				0.184
4.3	1.75			40	17.4	10.0	7.2	
4.4	2.00	67	0.38	31	21.1	11.2	8.1	0.148
4.6	2.50	74.9	0.58		19.8	11.4	8.1	0.188
5.0	1.00	32.3	0.08	80	28.3	16.6	10.7	0.085
5.2	1.50	64	0.30	29	14.8	10.8	7.3	0.133
5.3	1.75			16				
5.4	2.00	66.4	0.42	20	13.9	10.0	7.0	0.275

Table I Continued.

Sample Number	Draw Ratio	Fil Effic %	Press In.Wa.	Fraizer CFM	MAX μM	MFP μM	MIN μM	Packing Density
5.6	2.50	81.1	0.68	13				0.185
6.0	1.00	44.5	0.10	84	25.1	16.2	10.6	0.087
6.2	1.50			35				0.118
6.4	2.0	73.7	0.50	22	18.2	10.1	7.1	0.154
6.6	2.5	78.1	0.60	19	16.5	9.2	6.4	0.156
7.0	1.00	15.7	0.02	162	40.5	24.2	16.5	0.168
7.2	1.50	19.8	0.05	121				0.169
7.3	1.75				30.6	19.4	13.6	
7.4	2.00	19.2	0.06		29.6	18.5	12.8	0.163
7.5	2.25	28.0	0.12	66	22.1	17.0	9.7	0.184
7.6	2.50	29.1	0.12	90	38.0	17.4	12.7	0.267
8.0	1.00	13.8	0.02	163	20.8	14.4	10.9	0.145
8.2	1.50	13.1	0.04	129	45.3	20.6	14.3	0.156
8.3	1.75			96	29.2	18.9	12.9	
8.4	2.00	21.8	0.08	96	32.2	17.8	12.9	0.190
8.5	2.25			83	28.7	18.1	13.0	
8.6	2.50	17.8	0.08	85	37.1	17.4	11.7	0.156
8.8	3.00	22.3	0 0.08	98	33.3	19.2	13.2	0.181
9.0	1.00	14.3	0.02	178				0.174
9.2	1.50	13.3	0.04	144				0.053
9.3	1.75			115	32.2	20.9	13.1	
9.4	2.00	17.7	0.04	116	37.2	21.2	14.8	0.158
9.5	2.25			94	30.0	17.5	12.6	
9.6	2.5	17.8	0.06	99	33.2	20.0	12.7	0.145
9.7	2.75			109	29.7	21.3	15.1	
9.8	3.00			97	28.8	18.7	12.6	
10.0	1.00	18.8	0.04	131	44.5	19.4	14.2	0.118
10.2	1.50	26.8	0.08	95				0.132
10.3	1.75			71	22.1	15.4	11.1	

Table I Continued.

Sample Number	Draw Ratio	Fil Effic %	Press In.Wa.	Fraizer CFM	MAX μM	MFP μM	MIN μM	Packing Density
10.4	2.00	31.3	0.11	74				0.131
10.5	2.25			73	20.0	15.1	10.7	
10.6	2.50	45.8	0.18	66				0.138
10.7	2.75			64				
10.8				66	18.8	13.6	10.0	
11.0	1.00	21.3		120	38.8	20.1	13.8	0.129
11.2	1.5	34.9	0.18	48	19.3	12.2	9.4	0.182
11.3	1.75			28	13.9	11.3	7.3	
11.4	2.00	54	0.36	27	17.1	11.3	8.7	0.210
11.5	2.25			26				
11.6	2.50	60.3	0.52	20	17.5	9.4	6.6	0.254
11.7	2.75			21	11.8	8.6	5.9	
11.8	3.00	60.2	0.54	20	11.5	8.7	5.9	
12.0	1.00	22.6	0.04	132	38.1	18.4	12.9	0.133
12.1	1.25			127	40.0	18.7	13.2	
12.2	1.50	33.4	0.14	71	23.1	14.2	9.7	0.136
12.3	1.75			58	21.2	12.6	9.0	
12.4	2.00	37.1	0.160	59				0.157
12.5	2.25			56				
12.6	2.50	36.5	0.180	60	22.3	13.8	10.1	0.114
12.7	2.75			55	16.0	12.0	8.8	
13.0	1.00	23.8	0.060	114	31.8	18.6	13.1	0.116
13.1	1.25		113	21.7	17.4	12.9		
13.2	1.50	30.0	0.080	79	22.6	15.4	11.2	0.126
13.3	1.75			76				
13.4	2.00	28.7	0.120	69	22.7	13.7	9.20	0.150
13.5	2.25			73				
13.6	2.50	50.1	0.180	53	23.8	13.0	9.30	0.136
13.7	2.75			69	18.8	12.4	9.20	

Table I Continued.

Sample Number	Draw Ratio	Fil Effic %	Press In.Wa.	Fraizer CFM	MAX μM	MFP μM	MIN μM	Packing Density
13.8	3.00			66	22.0	13.1	9.20	
14.0	1.00	43.2	0.080	83	19.3			0.091
14.1	1.25			45	13.5	9.7	6.90	
14.2	1.50	74.1	0.380	28	14.0	8.4	6.2	
14.3	1.75			18	10.4	7.3	5.1	
14.4	2.0	77.4	0.70	17				0.206
14.5	2.25			13	9.1	7.0	4.5	
14.6	2.50	80.2	0.72	16	10.8	6.8	5.4	0.216
15.0	1.00	45.6	0.10	83	17.9	14.3	10.6	0.116
15.1	1.25	58.1	0.20	56	13.5	9.7	7.4	0.140
15.2	1.50	85.8	0.80	15	9.8	6.9	4.6	
15.3	1.75			9	7.2	5.4	3.3	0.231
15.4	2.00	89.2	1.48	7	7.7	5.4	4.2	0.279
16.0	1.00	46.8	0.08	86	20.1	14.5	9.6	0.092
16.1	1.25			56	20.6	13.4	9.7	
16.2	1.50	62.7	0.24	40	18.1	9.6	7.1	0.119
16.3	1.75			36	15.7	8.9	7.0	
16.4	2.00	63.4	0.24	34	12.0	9.1	6.3	0.120
16.5	2.25			38	14.8	9.3	6.6	
17.0	1.00	51.9	0.12	71	26.4	16.0	10.8	0.140
17.1	1.25	54.3	0.180	70	19.7	13.3	9.6	0.101
18.0	1.00	53.7	0.12	71				0.095
18.1	1.25	54.2	0.18	55	17.0	13.1	8.7	0.108
18.2	1.50	65.3	0.28	34	18.3	9.7	6.9	0.123
18.3	1.75			25	15.1	9.4	66.6	
18.4	2.00			28				
19.0	1.00			73	31.3	16.0	11.1	
19.1	1.25	53.9	0.16	62	18.9	15.1	10.2	0.100
19.2	1.50	42.0	0.12	67	21.4	13.8	9.9	0.104

Table I Continued.

Sample Number	Draw Ratio	Fil Effic %	Press In.Wa.	Fraizer CFM	MAX μM	MFP μM	MIN μM	Packing Density
19.4	2.00	52.1	0.14		23.2	13.7	9.6	0.132
20.1	1.25	54.6	0.14	75	19.0	12.8	9.3	0.103
20.2	1.50			50	22.2	13.7	9.7	
20.3	1.75	68.7	0.32	31	16.0	9.9	7.1	0.127
21.0	1.00	20.0	0.02	127	31.8	20.3	14.2	0.104
21.2	1.50	31.2	0.08	94	25.0	15.8	10.8	0.121
21.3	1.75			72				
21.4	2.00	37.8	0.10	73	22.5	15.0	10.1	0.138
22.0	1.00	23.0	0.04	124	24.3	19.4	13.4	0.114
22.1	1.25	19.8	0.06	103	24.7	18.3	12.7	0.137
22.2	1.50	26.7	0.08	90	24.6	17.0	12.4	0.141
22.3	1.75	30.7	0.08	78	21.7	15.7	11.2	0.138
23.2	1.50	24.9	0.06	112	22.2	17.5	13.0	0.131
24.0	1.00	22.8	0.04	136	26.2	19.5	14.0	
24.2	1.50	26.4	0.06	101	20.9	16.2	12.2	
24.3	1.75	31.2	0.08	91	27.0	19.8	12.8	
24.4	2.00	26.6	0.06	84				
24.5	2.25			80				
25.0	1.00	6.0			117.0	68		0.168
25.4	2.00	4.0			1.49	78.2		0.166

Table II. Processing and Performance Data on Selected Webs of Varied Fiber Diameters.

Sample Number	Air %	$\overline{Df}$ μM	Draw Ratio = 1				Draw Ratio = 2			
			P.D.	FET	MAX	MFP	P.D.	FET	MAX	MFP
14	90	3.2	0.095	43	19.3	15.4	0.206	77	9.6	7.1
15	90	3.9	0.110	45	17.9	14.3	0.275	89	7.9	5.6
5	85	4.0	0.085	32	28.3	16.6	0.262	66	13.9	10.0
11	80	5.5	0.129	21	38.8	20.1	0.210	54	14.7	9.6
8	70	8.5	0.145	14	20.8	14.4	0.179	22	32.2	17.9
7	70	9.9	0.163	16	40.5	24.2	0.168	19	29.6	18.4
9	70	8.8	0.172	14	33.0	20.6	0.163	18	37.3	21.2
25	60	18.5	0.168	6	117.0	68.0	0.166	4	149.0	78.2

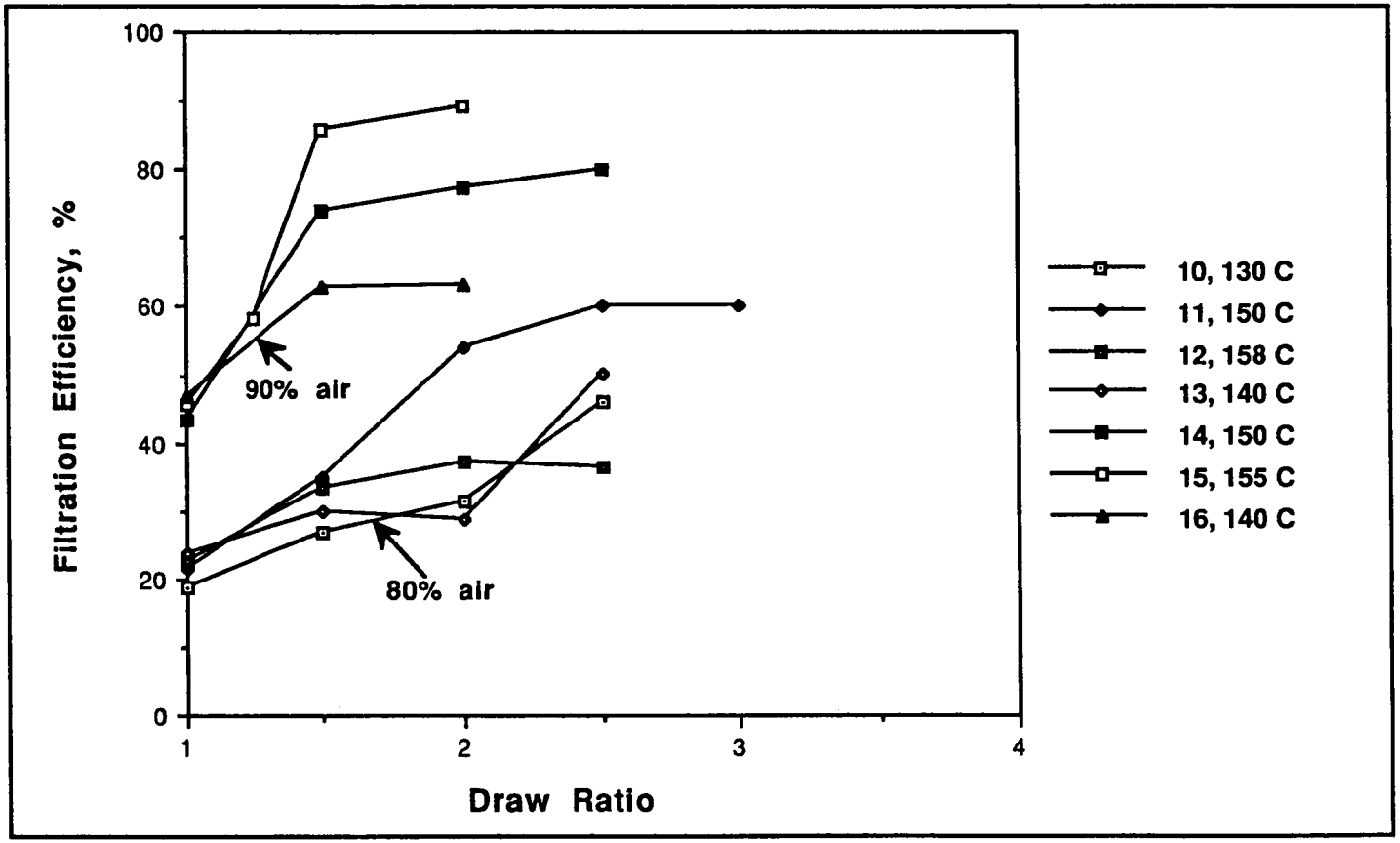


Figure 5.1 Particulate filtration capture efficiency due to hot draw post processing webs versus draw ratio for webs made at two air levels and processed at low strain rates and various oven temperatures.

to oven temperature, and draw ratio effects when processed at the lower range of strain rates. Each curve represents data for individual webs made at draw ratios of 1.0, 1.25, 1.5, 1.75, 2.0, etc. The gage length GL was assumed fixed so the strain rate ranged from (V2-V1) / GL where V2 ranged from V1 to about 3V1. As seen in Figure 5.1, the filtration efficiency for all the undrawn precursor control webs (i.e., draw ratio = 1.0) were below 50%. The ASTM 1989-15 test was run at the 10 cm/sec velocity level. This typically results in the most severe penetration of 1 micrometer monodisperse latex particulate. Processing the precursor webs made at the higher 90 % air level at progressively higher oven temperatures resulted in progressively higher efficiencies approaching 90% as draw ratios increased to 1.5. Additional increases in draw only created slight increases in the efficiency values for webs drawn at 150 and 155 C as seen in Figure 5.1. Precursor webs made at the lower 80 % air level showed varied effects at the different levels of oven processing temperature. Progressive increases in efficiency were observed for 130 through 150 C. However, the 80% air webs drawn at 155 C. showed no improvement in efficiency beyond the 50% stretch level (draw ratio 1.5). This filtration efficiency curve flattens in a way similar to the 140 C. curve for the high 90% air precursor web. This flattening in the capture efficiency response with draw may be the result of a deficiency in the forces producing buckling whereby the compacting forces resulting from tension are matched by the bending resistance of the larger filaments dispersed within the web.

The 80% air precursor processed at 150 C exhibited linearly increasing efficiency up to three times its unconsolidated or control value. Low temperature processing of the low air webs produced capture efficiency increases from 22% up to 50% over a 150% strain range.

Figure 5.2 illustrates similar effects of temperature, air rate, and draw ratio effects which occur when processing the same precursor webs at high strain rates equal to three times (3X) the lower strain rates. At all precursor webs, webs ruptured if processed beyond draw levels of 2.0 or a 100% extensional strain.

For the high air precursors, it was found that processing the web at 130 C produced decreases in the capture efficiency. This reflects a lower limit of processing temperature at which the polypropylene polymer was not adequately softened to consolidate. Processing at 140 and 150 C and high strain rates produced efficiency levels less than these respective oven temperatures at the lower strain rates.

The lower 80% air level precursor webs exhibited similar degradation in the capture efficiency enhancement at the 3X processing strain rates. None of the high strain rate (3X) processed webs had efficiencies greater than the 140 C webs made at the lower strain rate.

Processing Tensile Modulus

The equilibrium tension existing in the web during hot draw processing

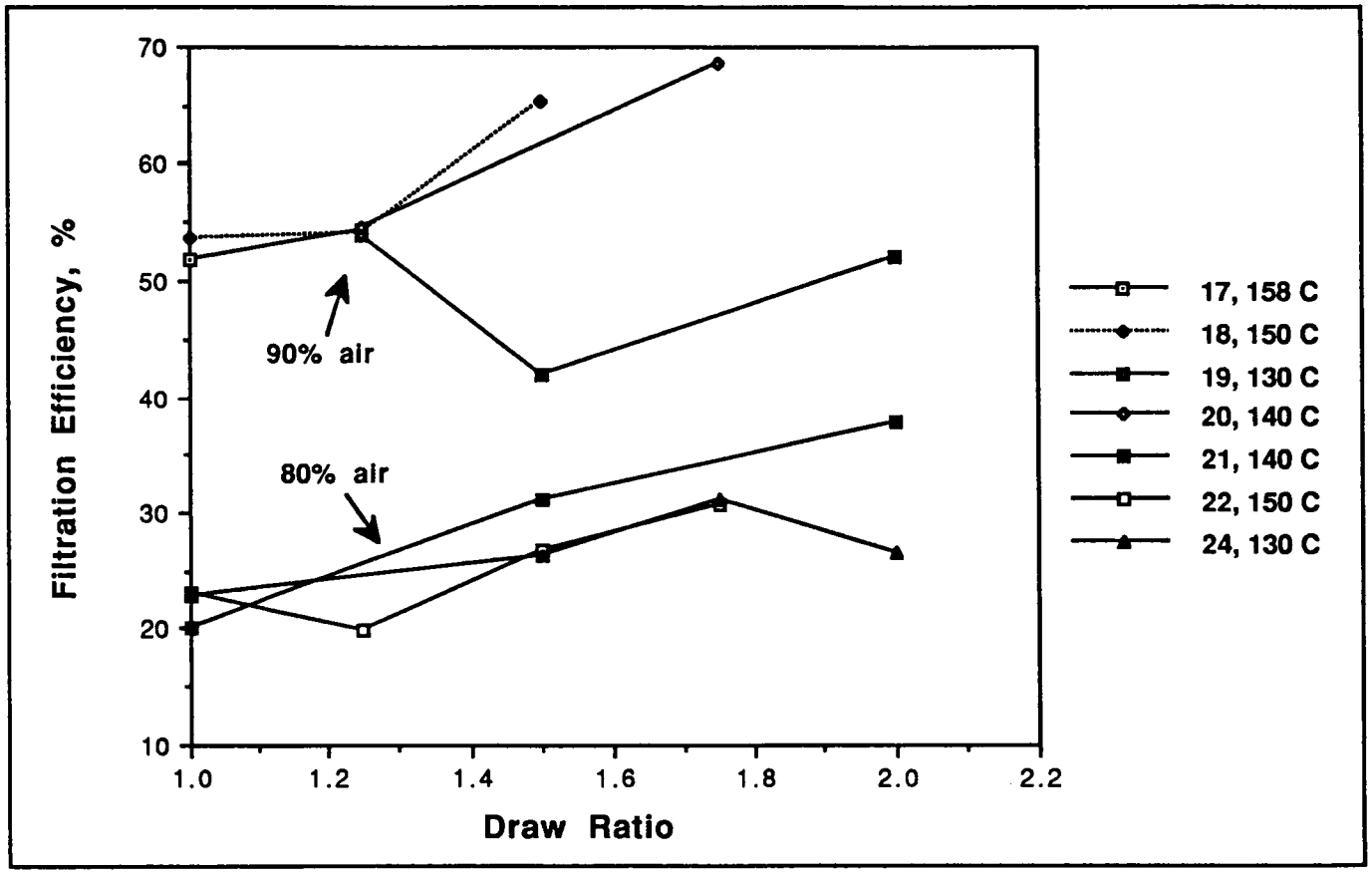


Figure 5.2 Particulate filtration capture efficiency due to hot draw post processing webs versus draw ratio for webs made at two air levels and processed at high strain rates and various oven temperatures.

was predicted to affect the degree of consolidation. Each curve in Figure 5.3 is a plot of the steady state tensile load that developed while processing the particular precursors at the draw ratios up to 1.75. As an example, the curve having the lowest slope was a harsh web processed at 150 C. at low strain rates. The slope of the curve is directly related to the tensile modulus during the steady state processing. In general, the equilibrium processing tension increased with decreasing processing oven temperature (T in the figure legend), increasing extensional strain and strain rate (R), and increasing air level (A) to make the precursor web. The letters H, M, and L in the legend indicate high, medium and low levels respectively. The theory outlined in chapter 3 implied that the effect of tensile modulus in the Euler buckling relationship was indeterminate. The experimental results separated into groups according processing strain rate. This is probably due to the thoroughness of web filament heating effected by the combination of oven temperature and web dwell time in the fixed length oven. Considering only the webs processed at high air and low strain rates, (samples 15, 14, and 16) the webs display processing tension levels which were reciprocally related to increases in filtration efficiency shown in Figure 5.1. Higher efficiencies were associated with greater processing temperature for the high air precursor webs. For these precursors, the higher temperature processing created the greater consolidation for filtration. Consolidated webs from 80% low air precursors displayed optimum capture efficiencies at the lower 150°C processing temperature

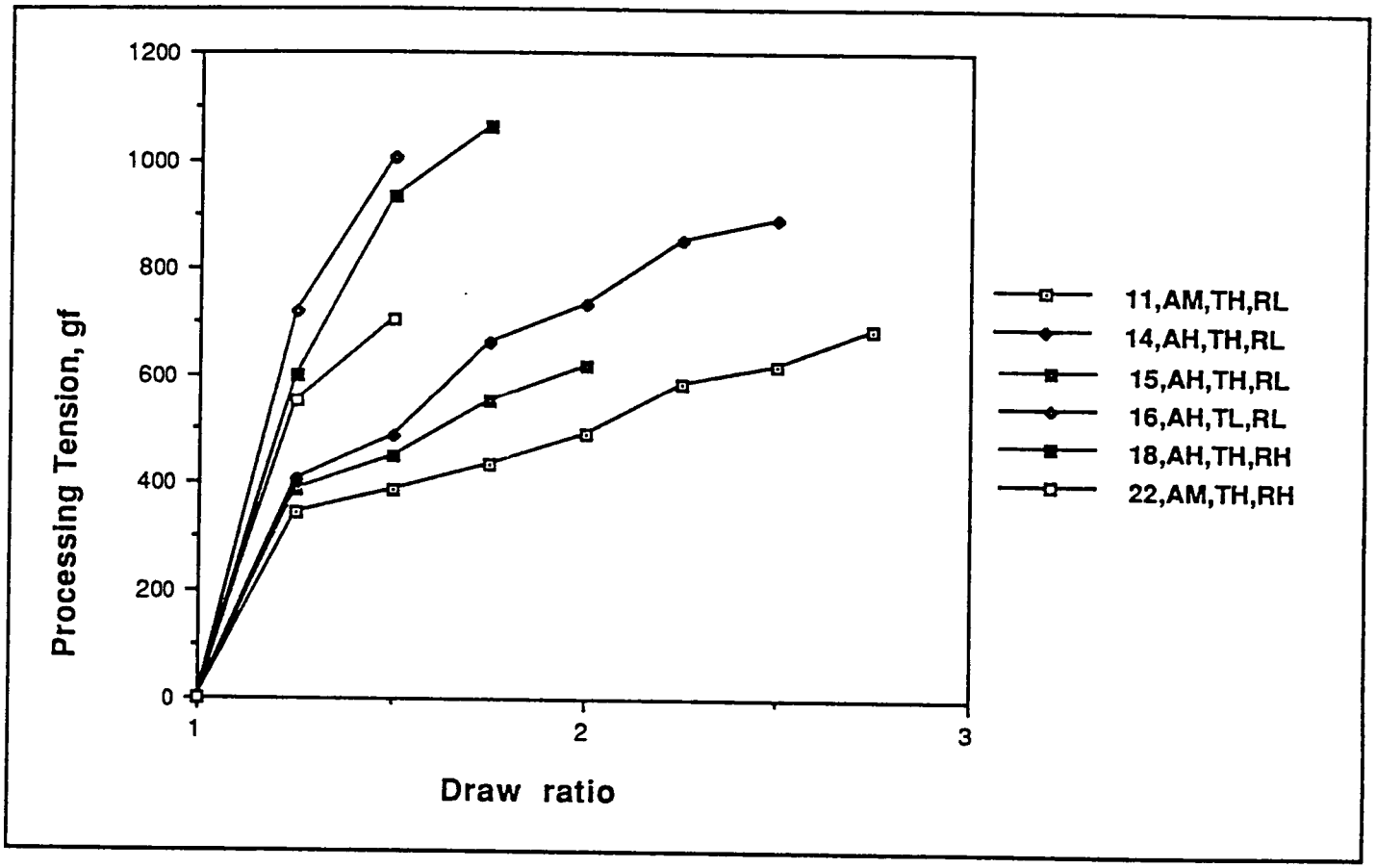


Figure 5.3 Plots of tensile stress in webs during draw processing versus draw ratios at high (H), medium (M) and low (L) levels of precursor air level, and post processing temperature and strain rate.

indicating that the rheological nature of this precursor web required less temperature to effect web alteration for maximum filtration capture efficiency. The specific structural consolidation that caused the enhanced efficiencies is discussed relative to pore size changes below.

Bonding Level Effects

Two sets of precursor webs made at 85 and 70% processing air levels and three levels of web bonding per set were processed at the low strain rate levels and 150° C. The levels of bonding in the web designated as high (H), medium (M), and low (L) were quantified by the magnitude of breaking strain observed in room temperature tensile tests of the precursor webs. Figure 5.4 illustrates the differences in filtration efficiency of processed webs consolidated at various draw ratios due to differences in filament bonding in the precursor webs. The differences in bonding levels had no consistent effect on high or low air precursor webs at any draw ratio.

The post drawn webs originating form precursor webs made at high 85% process air levels exhibited characteristic increases in filtration capture efficiency, but those made at low 70% processing air levels exhibited almost no enhancement in capture efficiency due to hot draw processing up to 150% strain level. The effect of the bonding differences on processing was negligible.

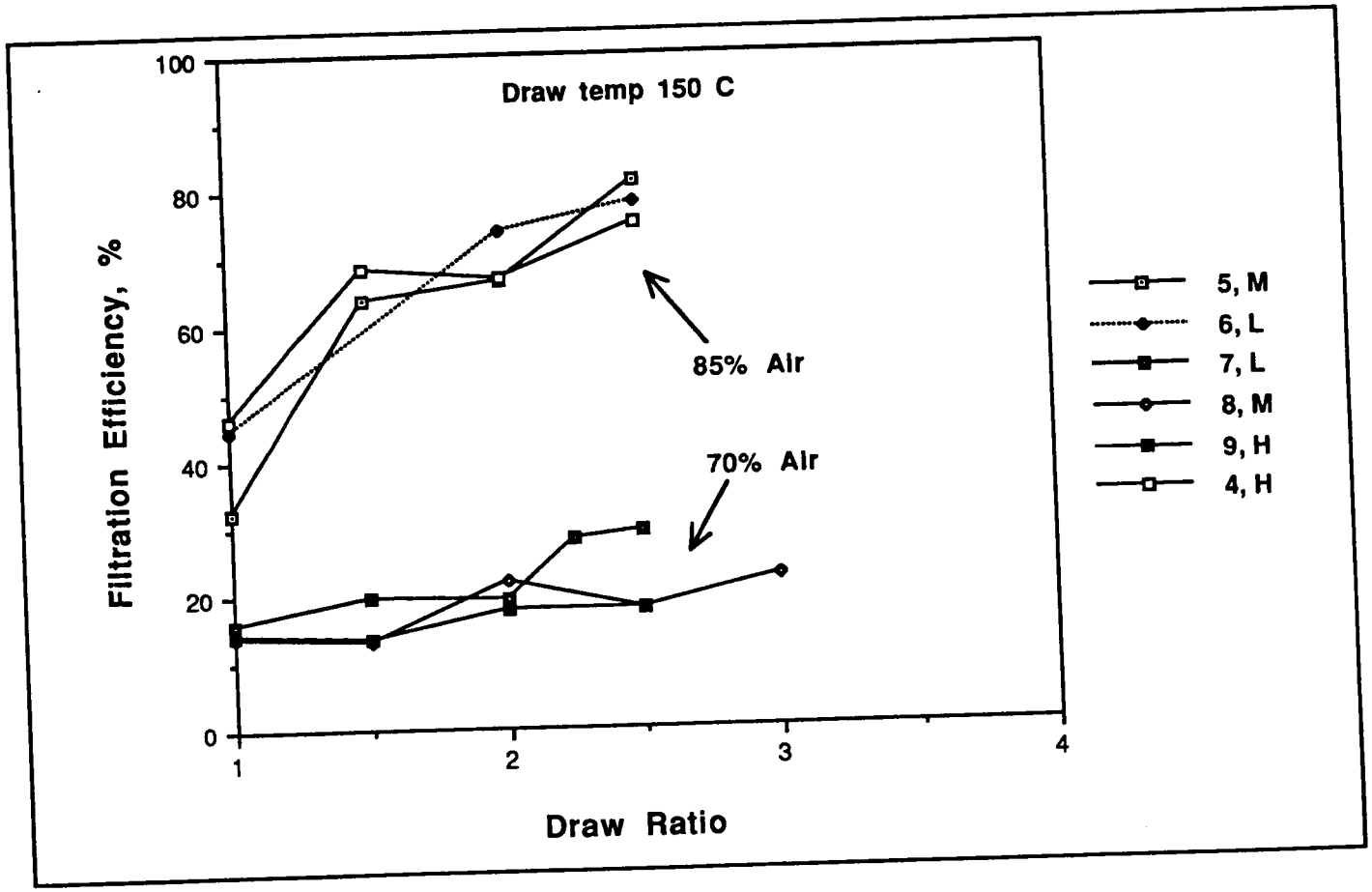


Figure 5.4 Particulate capture efficiency versus post processing draw ratio for webs consolidated from precursor webs having three levels of fiber bonding: L is low; M is medium, and H is a high level of bonding.

Air Permeability

The fluid permeability of the drawn webs is a primary attribute of filtration performance of filter media. Frazier air permeability values versus post processing draw ratio of the consolidated webs (sample 4 to 16) are plotted in Figure 5.5. Web permeability generally decreases rapidly with drawing up to a draw ratio near 1.5 then continues to decrease slowly with increases in draw ratio. The relationship between filtration performance versus air permeability data was best expressed in terms of the penetration values given by the quantity $(1 - \eta)$ for the collection of samples as shown in Figure 5.6. One point to note is that the ratio of these performance parameters holds in general for drawn and undrawn webs. This suggests that the general meltblown structure characteristics affecting particulate penetration and flow are preserved after restructuring the webs via post drawing. Air flow permeability is the reciprocal of flow resistance and resistance directly relates to particulate capture efficiency based on a pore size analogy. Structural changes effected by the post processing will be discussed below.

Values of the overall filtration efficiency of webs computed using the Benjamin Liu equation Basic program did not agree with measured values. Computed penetration values for control undrawn webs were from 1.6 to 15 times smaller than the measured values. This variability could have been due to the wide difference in the family of webs. For the draw consolidated and highly compacted webs, the computed values were from 4 to 6000 times

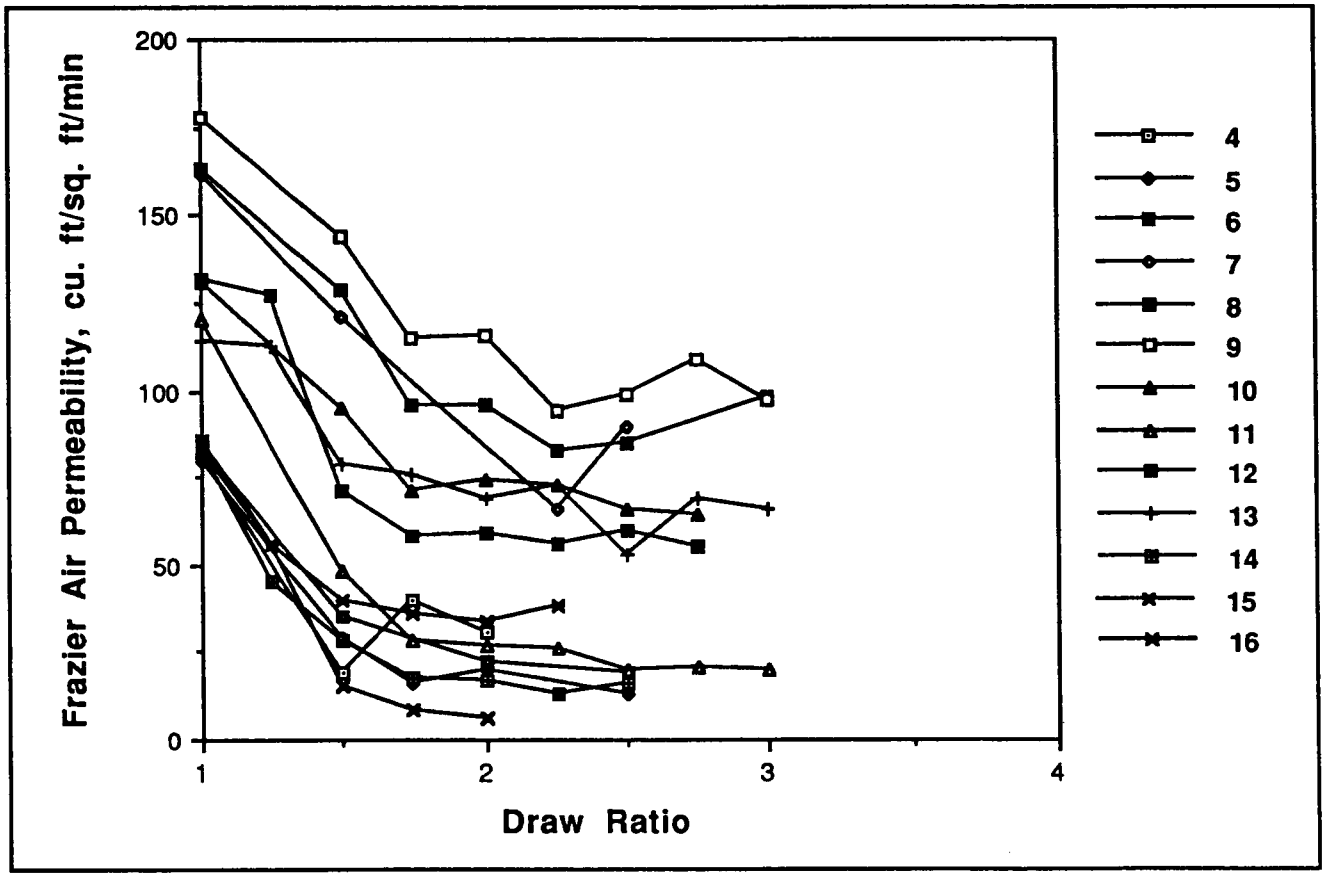


Figure 5.5 Plot of Fraizer air permeability versus post processing draw ratio for the consolidated webs.

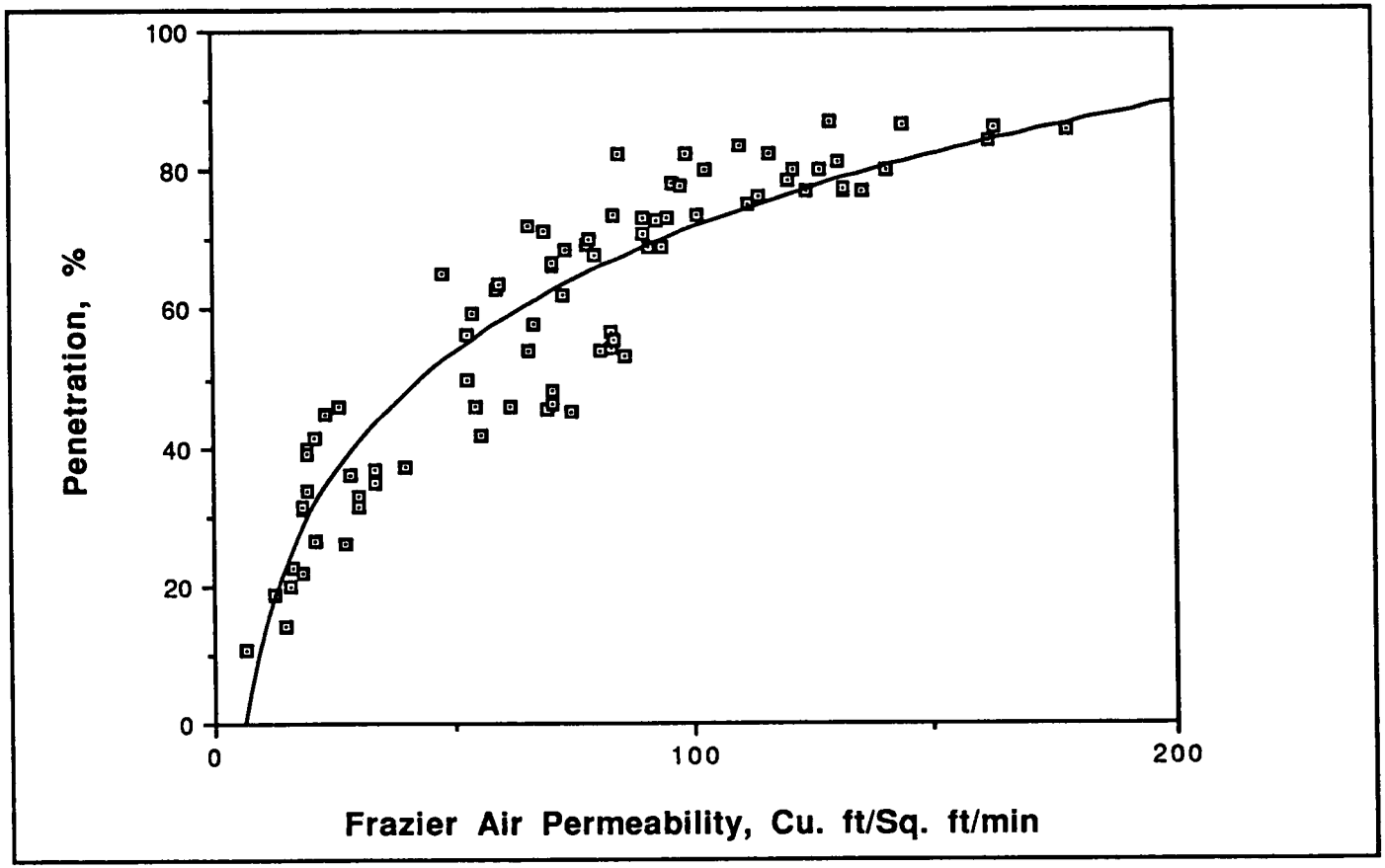


Figure 5.6 Particulate penetration values versus air permeability data for the entire collection of samples.

the measured values. A possible explanation is that the high packing densities produced by consolidation was very uncharacteristic of Liu's web set which were made by natural forming forces on fibers on uniform diameter. The Liu equations also utilize an area factor of 1.6 used to adjust the computed results of his family of tested webs to his physically determined measures of filtration efficiency. This 1.6 factor probably involves some inherent relationship between fibers assembled by specific (natural) forming forces and the resultant packig density attainable.

Pore Size Distribution and Structural Changes

Pore size features of the processed webs were assessed using the various statistical measures of pore size distribution output from the Coulter Porometer. The so called "statistical measures" included the maximum pore size (MAX), mean flow pore size (MFP) and various number distributions. Figure 5.7 is an SEM photomicrograph illustrating a typical change in the filament orientation and pore structure resulting from the hot-draw post processing. Figure 5.8 is a Porometer print out illustrating the distributions and changes in pore structure dimensions associated with the physical restructuring of filaments corresponding to two webs illustrated in Figure 5.7. It is noted that the printed values of the measures of pore size distribution for the processed sample are about one half those of the precursor web. Figure 5.9 is a

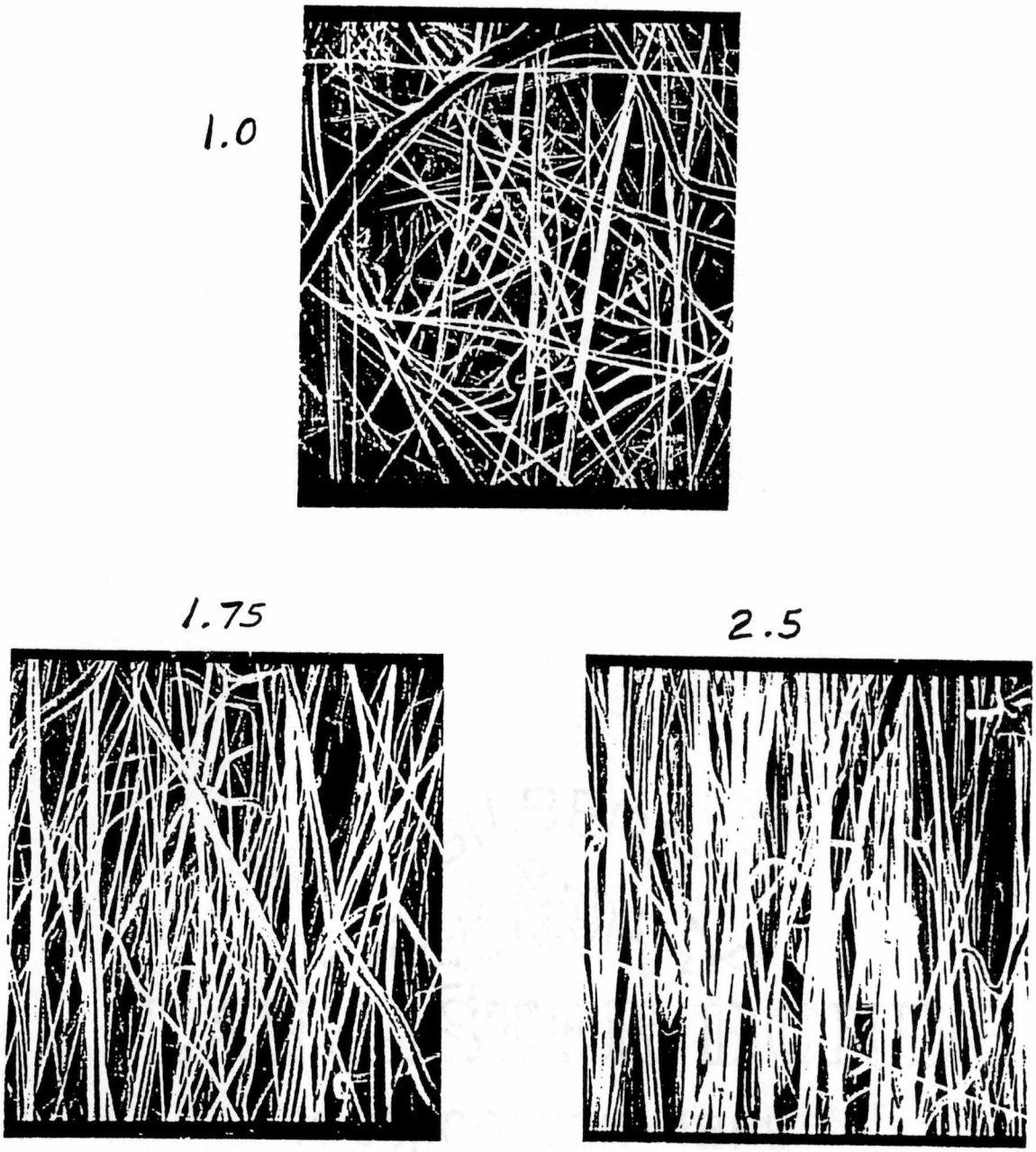


Figure 5.7 Scanning electron photomicrographs (SEM) illustrating typical changes in the filament orientation and pore structure of the precursor web (DR = 1.0) resulting from the hot draw processing at DR = 1.75 and at DR = 2.5.

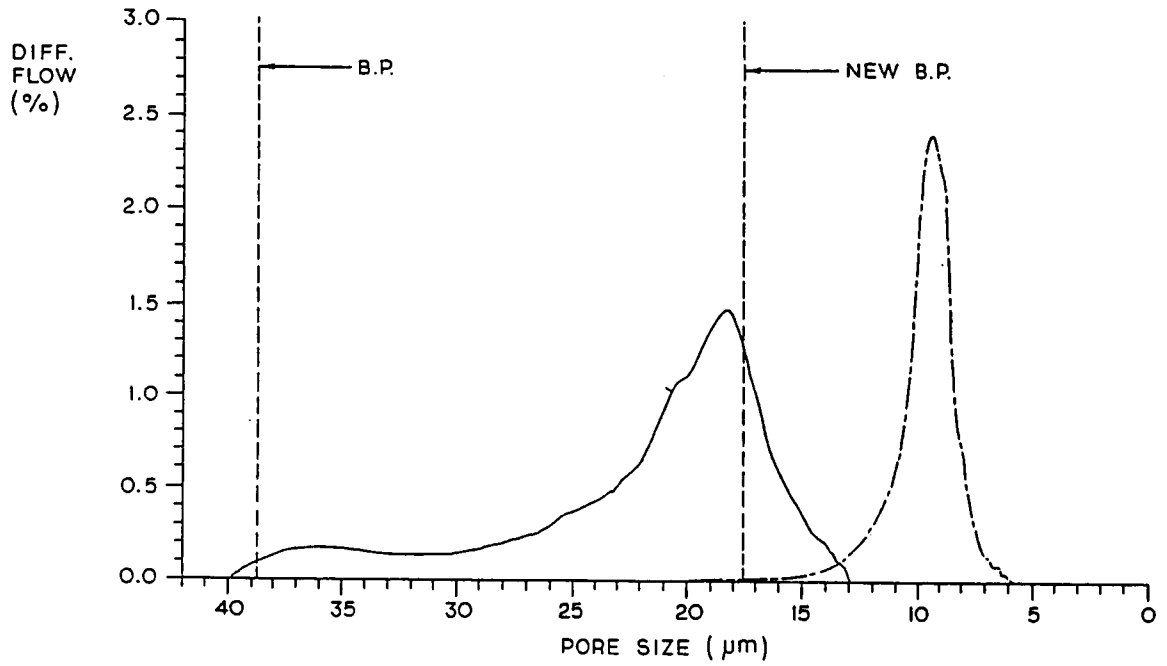


Figure 5.8 Porometer differential flow distribution print out for two webs: (a) a high air precursor web (DR = 1.0) , and (b) the web of (a) post draw processed to a DR = 2.5. Note the large changes in the pore structure measures associated with the respective physical restructuring of filaments as shown in Figure 5.7.

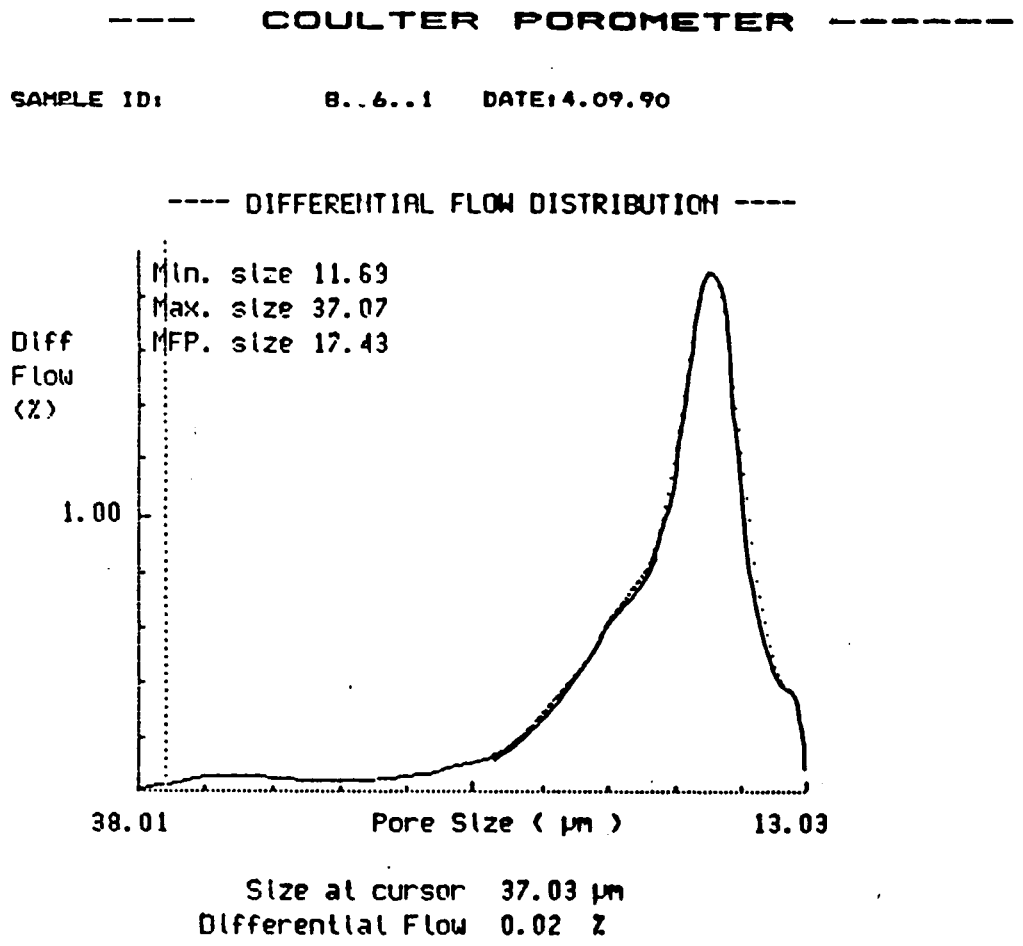


Figure 5.9 Porometer differential flow distribution print out of a web draw consolidated to a draw ratio of 2.5 from precursor web made at the lowest melt blowing air rate. These webs experienced virtually no performance benefits from post drawing up to 150% strain.

differential flow distribution print out from the Porometer (TN) instrument of a sample processed using precursor web made at the lowest experimental processing air. These webs experienced virtually no performance benefits from post drawing up to 150% strain. Negligible changes were also observed in the MAX and MFP values.

Figures 5.10 and 5.11 are plots containing maximum pore size (MAX) versus post processing draw ratio data for the webs made at the four levels of meltblowing process air. Respective plots for the mean flow pore measurements (MFP) are given in Figure 5.12 and Figure 5.13. The decrease in the pore size measures with draw ratio levels off at draw ratios beyond 1.5 (strains of 50%). This is close to the theoretical unidirectional strain for complete closure of the idealized processed unit cell. Further, for the webs processed from the higher air level precursors, the pore measures decrease rapidly between draw ratios between 1.0 and 1.5. The precursors made at the low 70% air level experienced negligible alterations in pore dimensions on hot draw processing. Figure 5.14 is a plot of web sample packing density versus processing draw ratio for webs processed at the lower range of strain rate. Packing density changes for any sample reflect the changes in filtration performance measures for individual samples, yet the packing densities alone do not relate to filtration performance measures for the collective sample set.

Bubble point or maximum pore size measures are traditional means for assessing filtration characteristics of filter media. Figure 5.15 is a plot showing

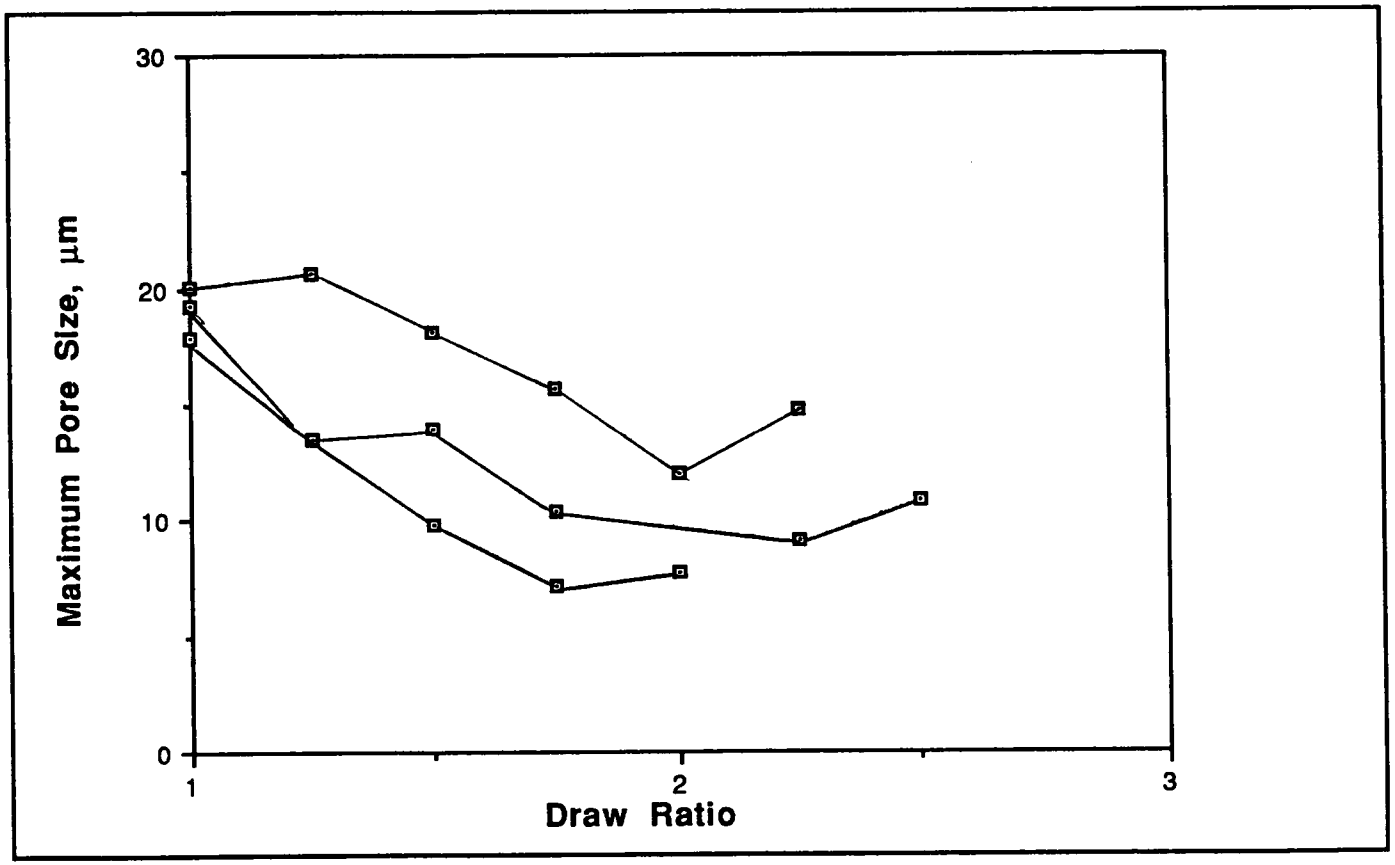


Figure 5.10 Plot of maximum pore size (MAX) versus post processing draw ratio for precursor webs made at 90% die air levels.

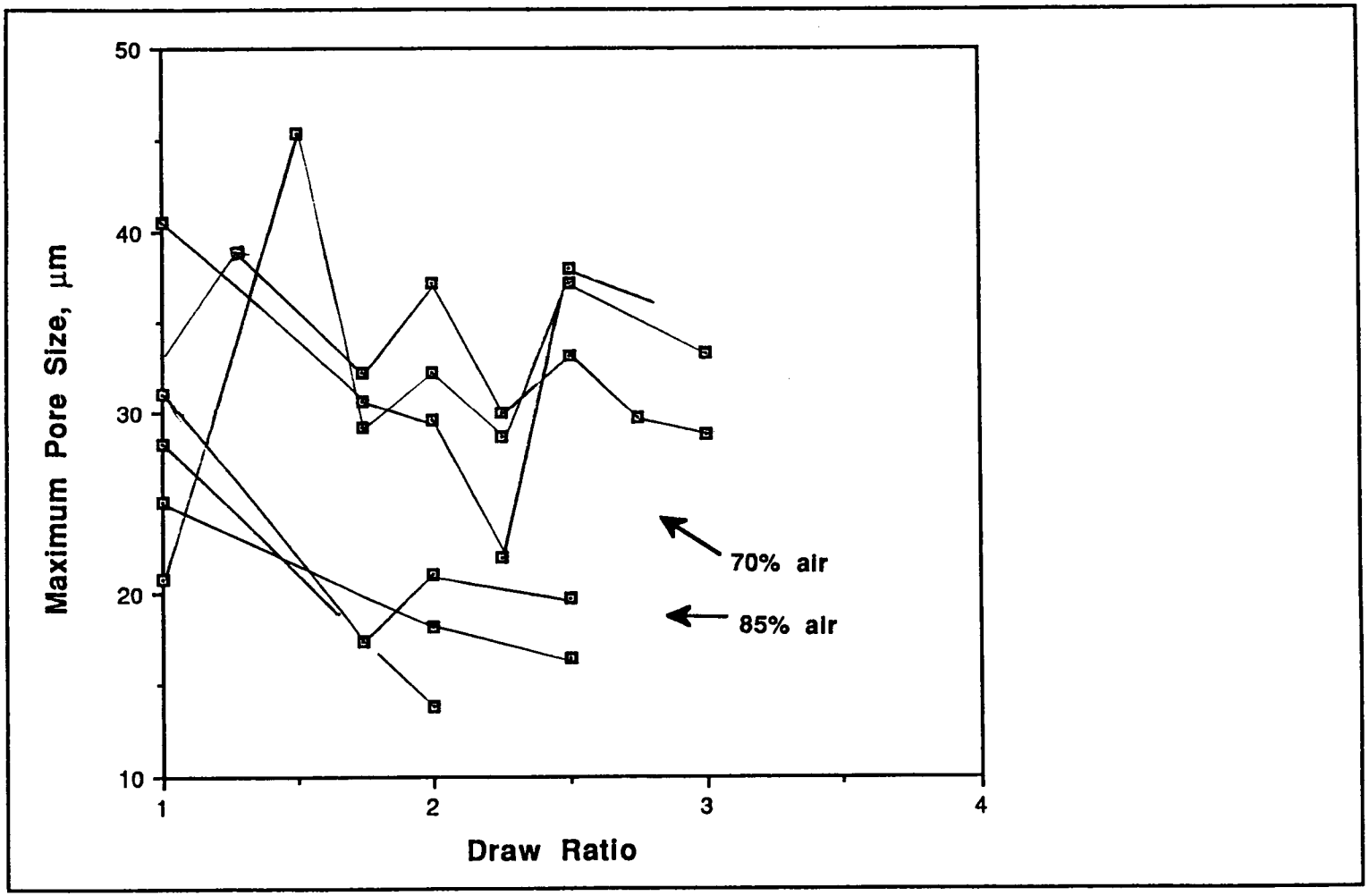


Figure 5.11 Plot of maximum pore size (MAX) versus post processing draw ratio for precursor webs made at 70 and 85% die air levels.

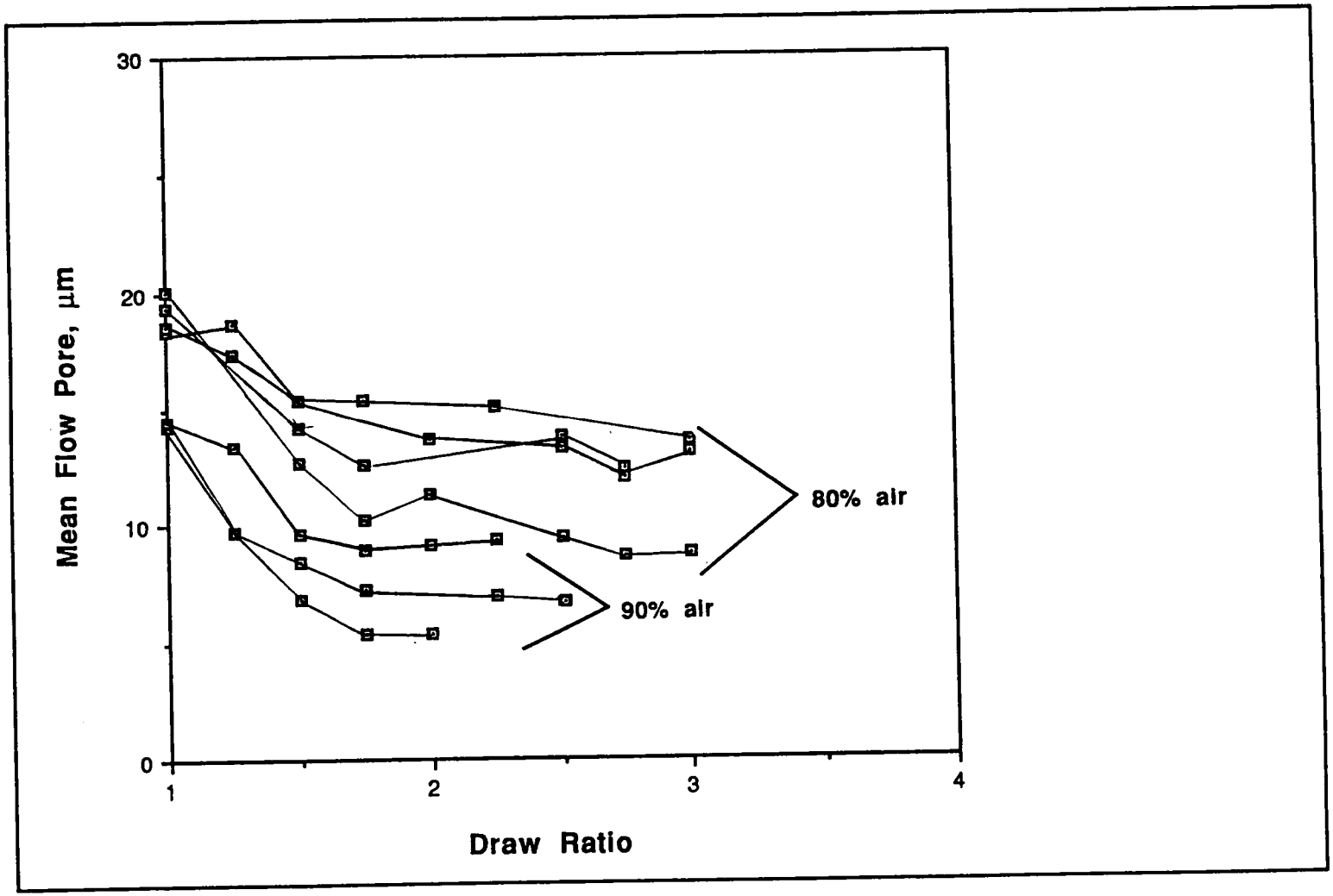


Figure 5.12 Plot of mean flow pore size (MFP) versus post processing draw ratio for precursor webs made at 80 and 90% die air levels.

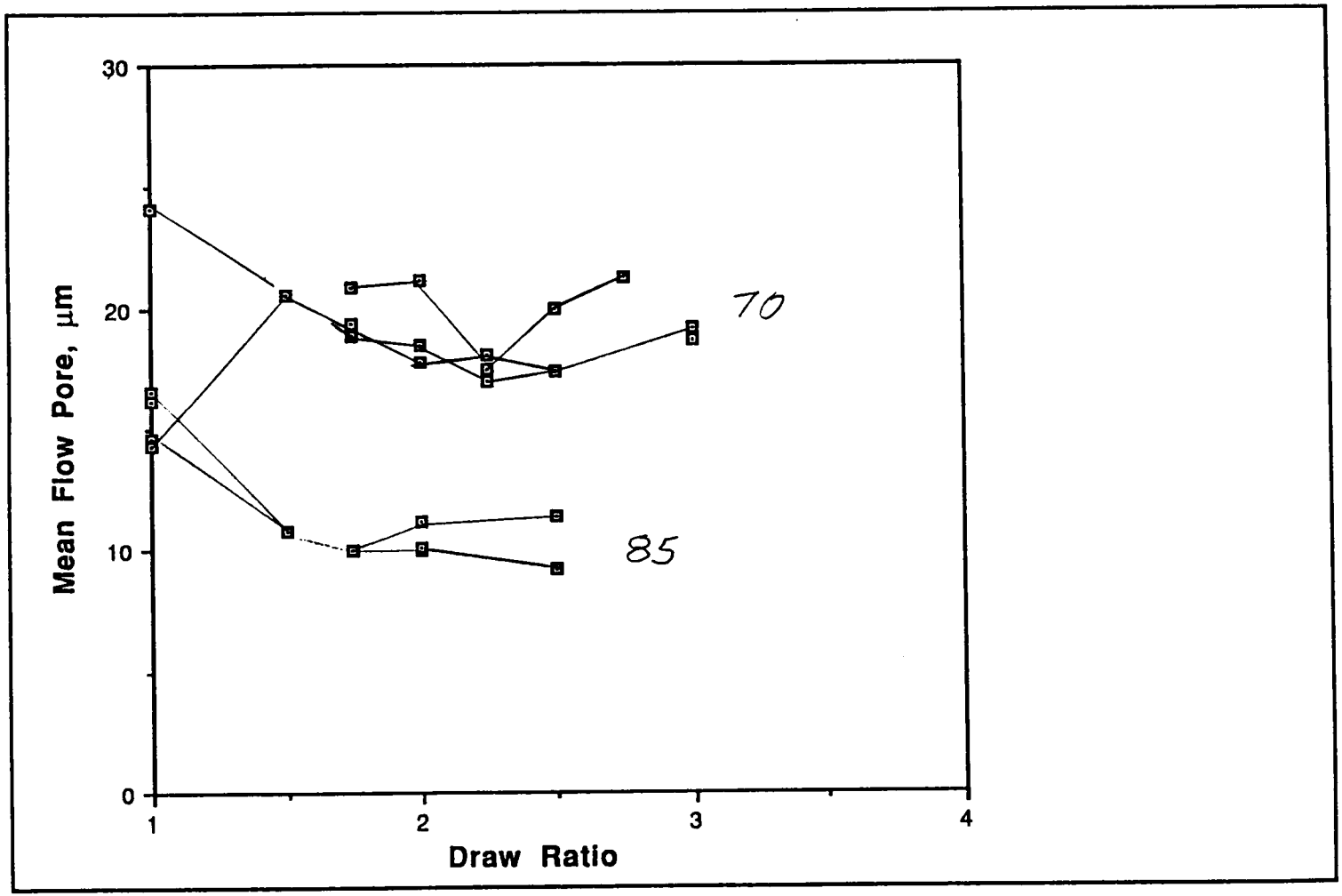


Figure 5.13 Plot of mean flow pore size (MFP) versus post processing draw ratio for precursor webs made at 70 and 85% die air levels.

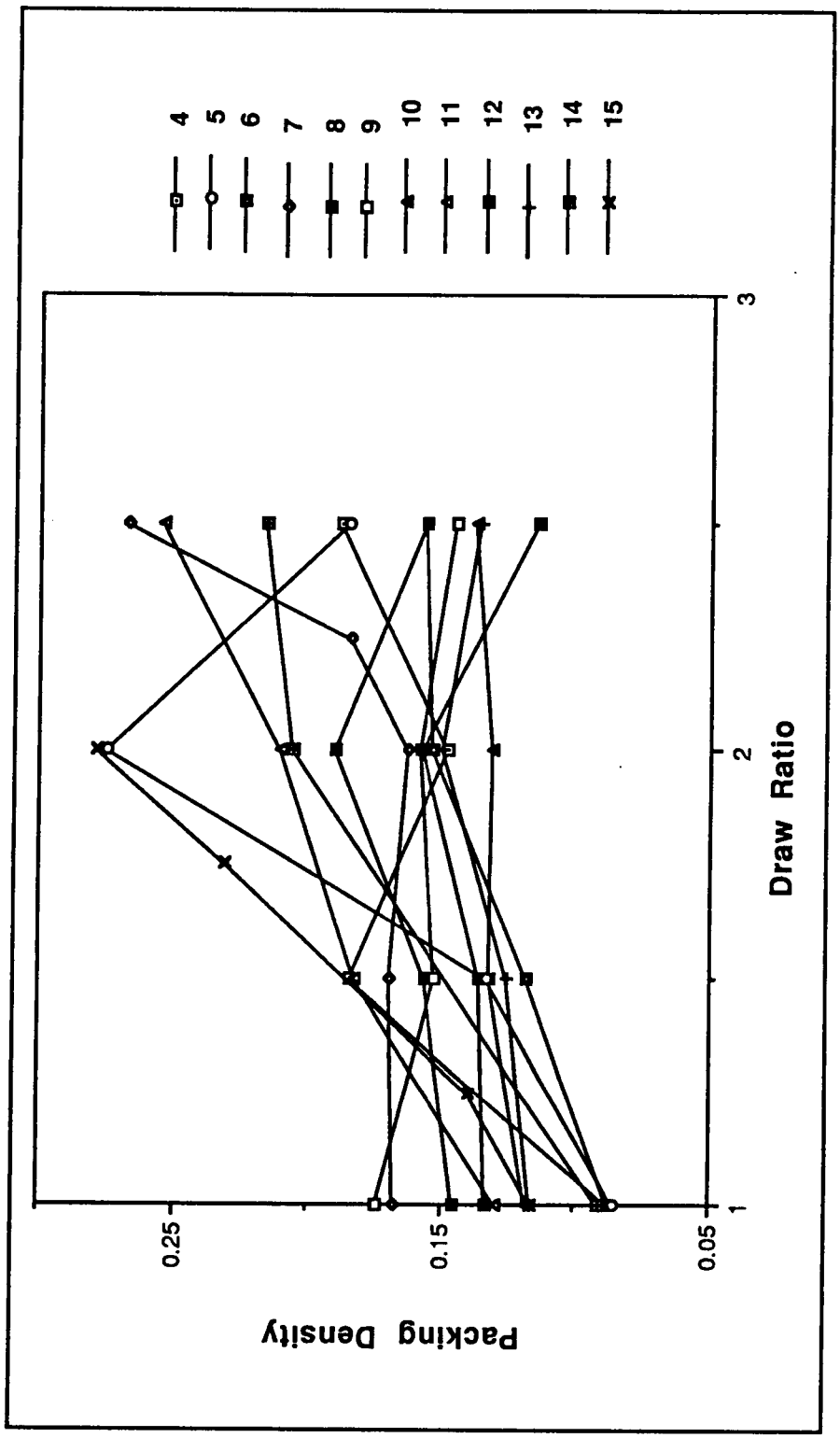


Figure 5.14 Plot of packing density versus draw ratio for webs post processed at low strain rates.

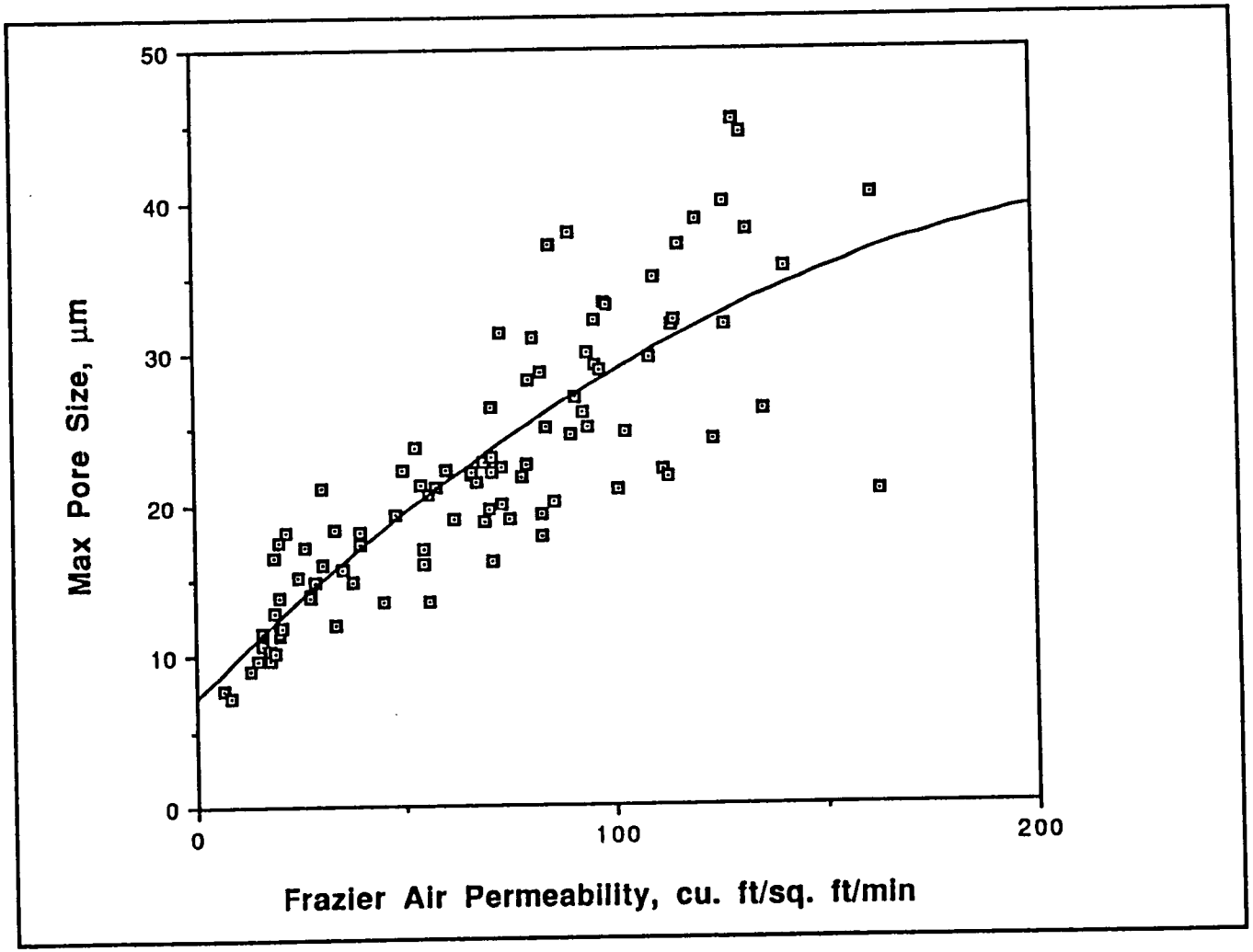


Figure 5.15 Plot of maximum pore size (MAX) for the collective web sample processed at a draw ratio of 2.0 versus Fraizer air permeability.

the relationship between the MAX and air permeability for the collective sample. Figure 5.16, 5.17 and 5.18 are plots of MAX, MFP, and packing density respectively, versus nominally 1 micron particulate penetration through the webs and illustrate the strong predictive value of the MAX and MFP measures to infer filtration performance. The relative goodness of fit indicates that MFP and the MAX are useful to predict the collective filtration performance of the webs compared to packing density. Packing density predicts subset performance behavior but not collective performance for the entire sample set.

Steric Effects of Fiber Size

The sample sets created from webs produced at varied processing air levels have differences in the average diameter of the constituent filaments as shown in Table I. Figure 5.19 is a plot of the process air level used for the precursor versus the average fiber diameter of the web. As the diameters of web filaments increase, the steric hinderance to forming or arranging such fibers into small pores typically increases for natural formation processes. Figures 5.20 and 5.21 are plots of MAX and MFP for undrawn precursors and post processed web counterparts drawn to a draw ratio of 2.0 versus the average fiber diameter of the constituent filaments in the webs. The curves for draw ratio equal to 2.0 parallel the curve of the undrawn webs for web fiber diameters beyond about ten micrometers. Thus, the draw processing provides the small pore forming benefit associated with "fine filaments webs" in a web

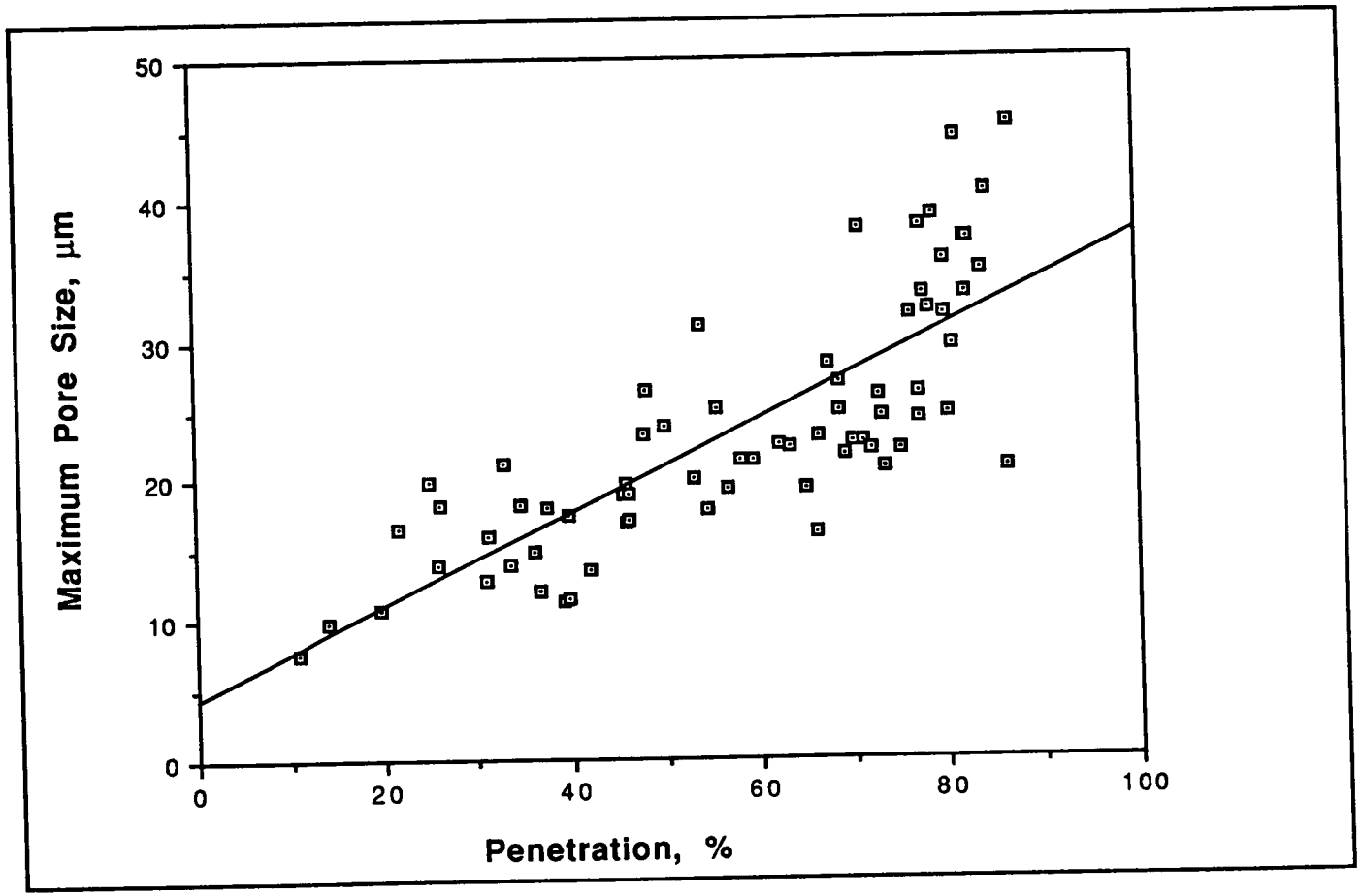


Figure 5.16 Plot of maximum pore size (MAX) for the collective web sample processed at a draw ratio of 2.0 versus particulate penetration.

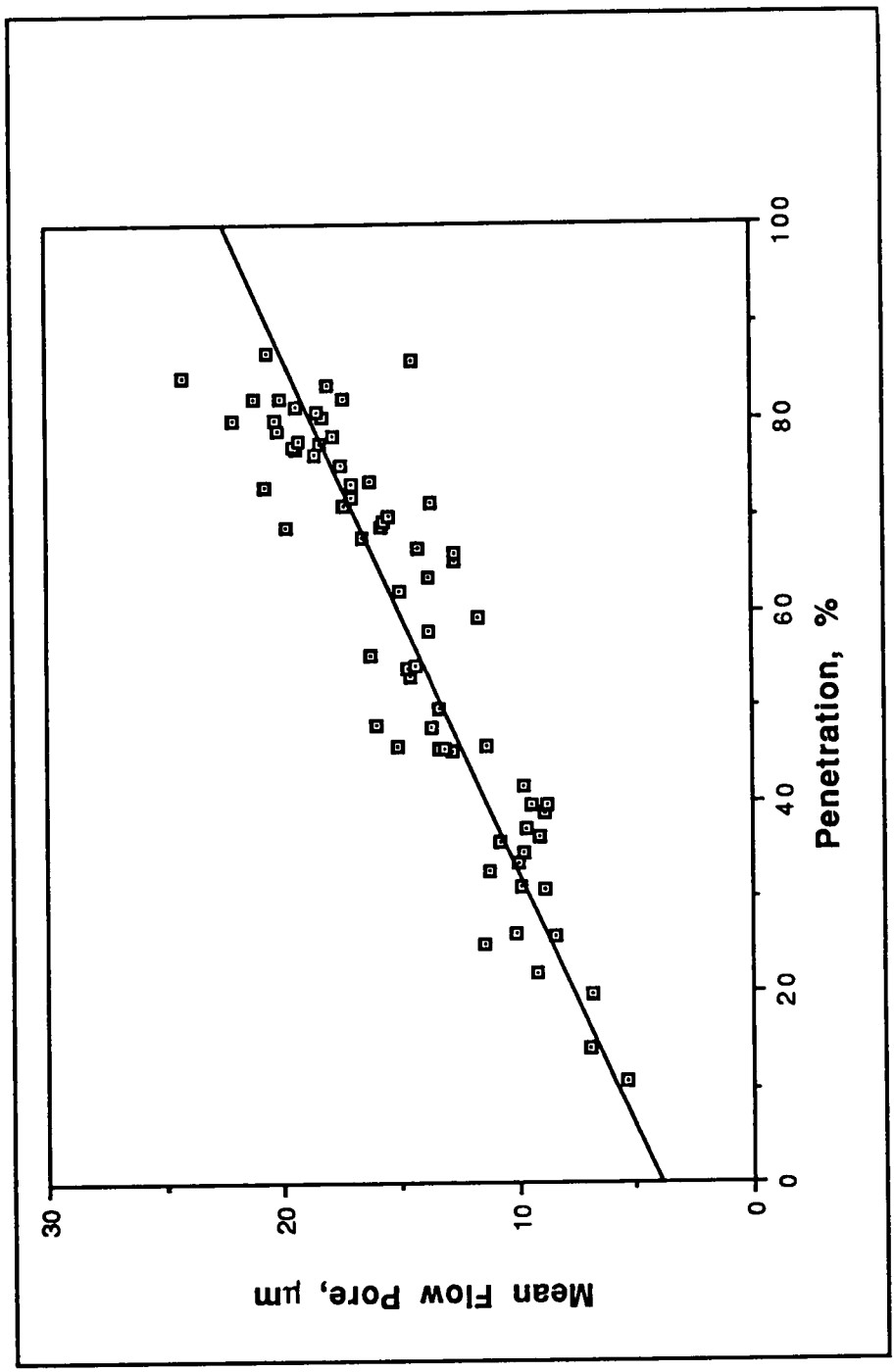


Figure 5.17 Plot of mean flow pore size (MFP) for the collective web sample processed at a draw ratio of 2.0 versus particulate penetration.

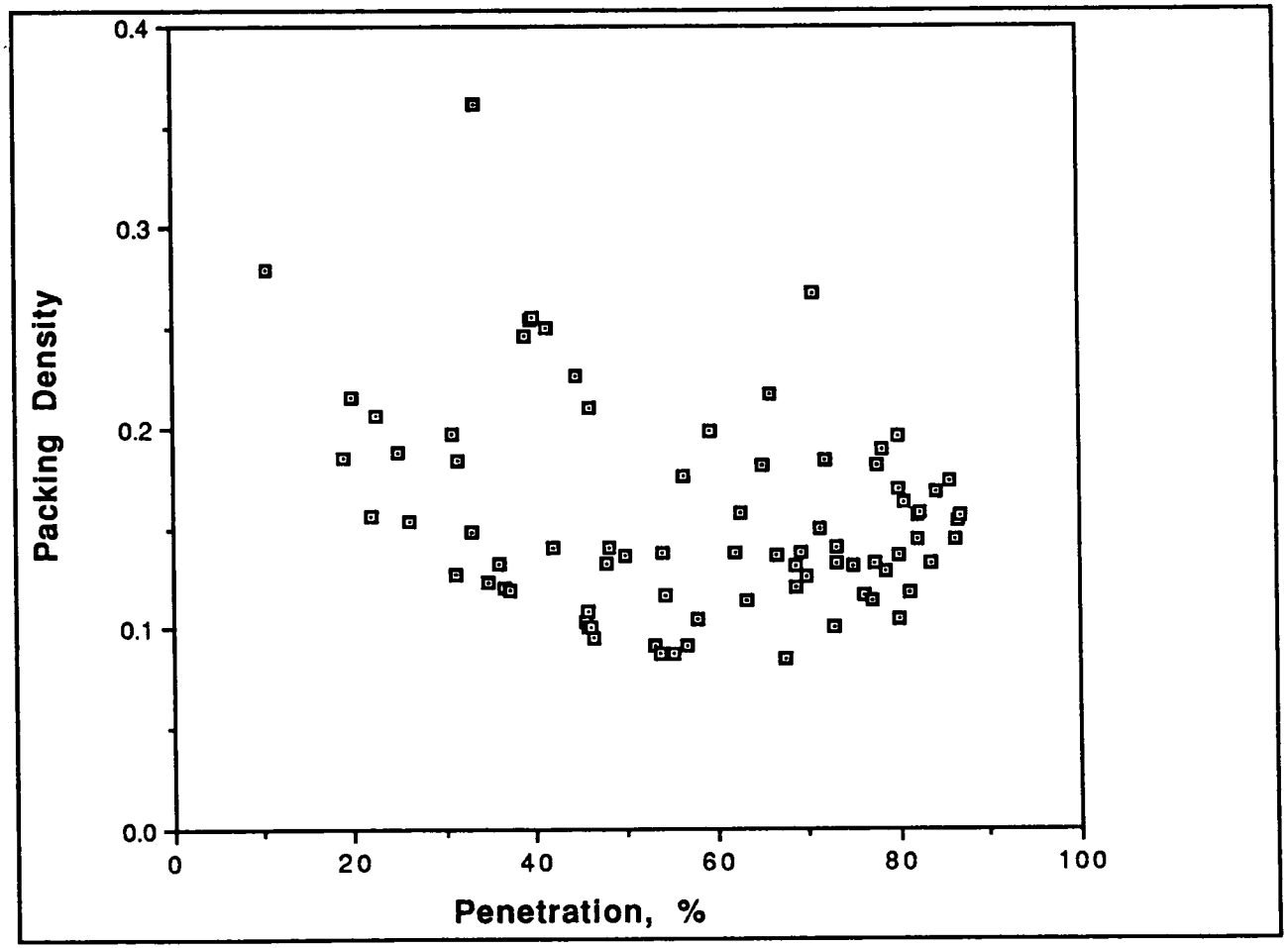


Figure 5.18 Plot of packing density for the collective web sample processed at draw ratio of 2.0 versus particulate penetration.

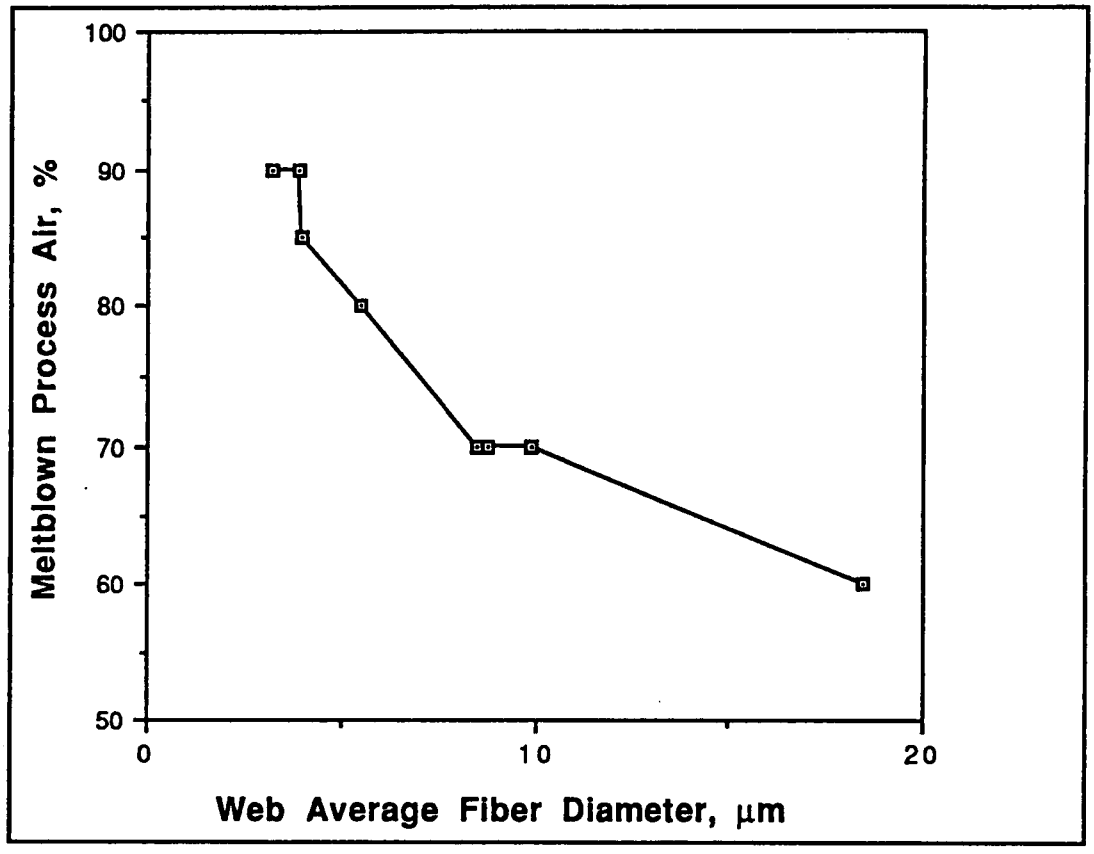


Figure 5.19 Plot of the primary air level used in precursor web production versus the average diameter of the fibers in the web.

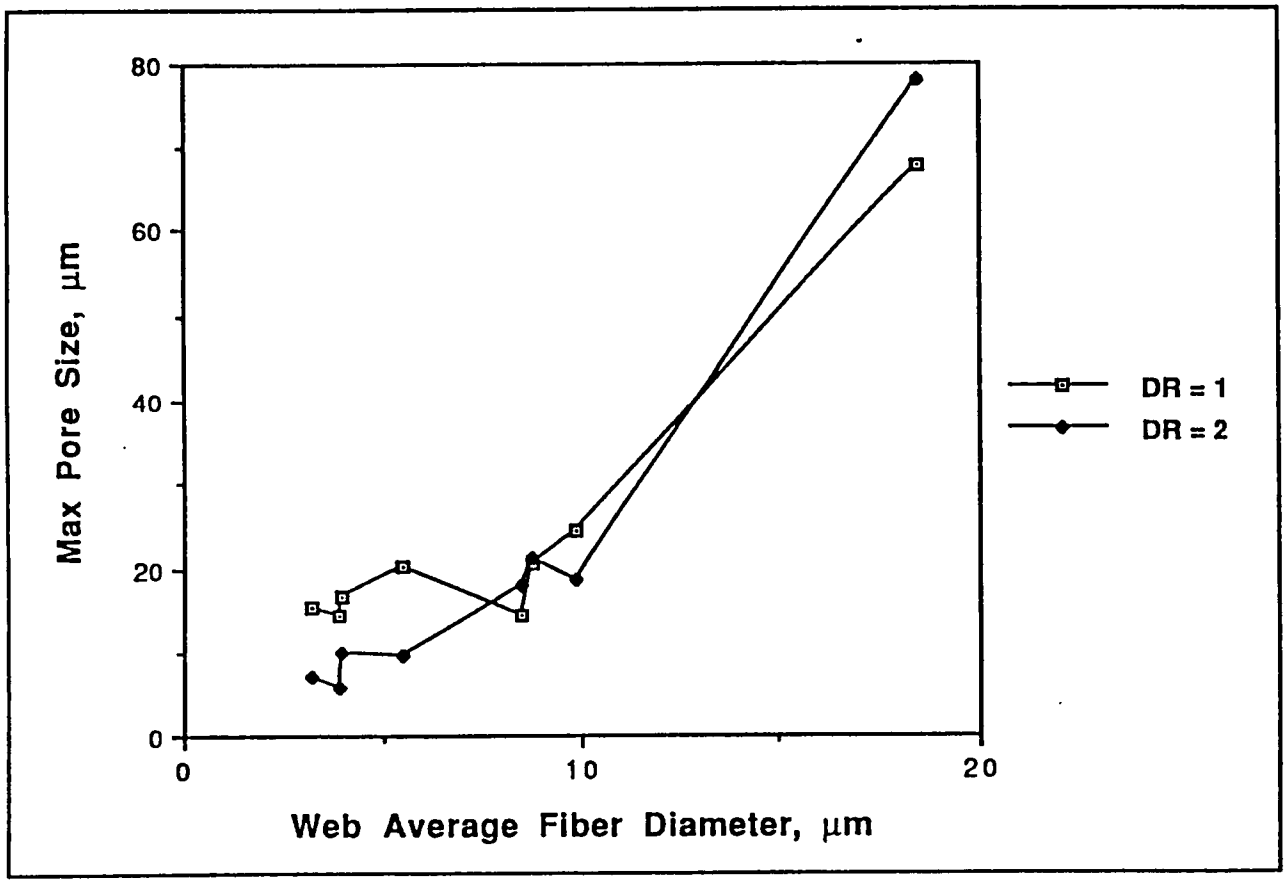


Figure 5.20 Plot of the maximum pore size (MAX) for precursor webs and counterparts post processed to DR = 2.0 versus the average diameter of fibers in the web.

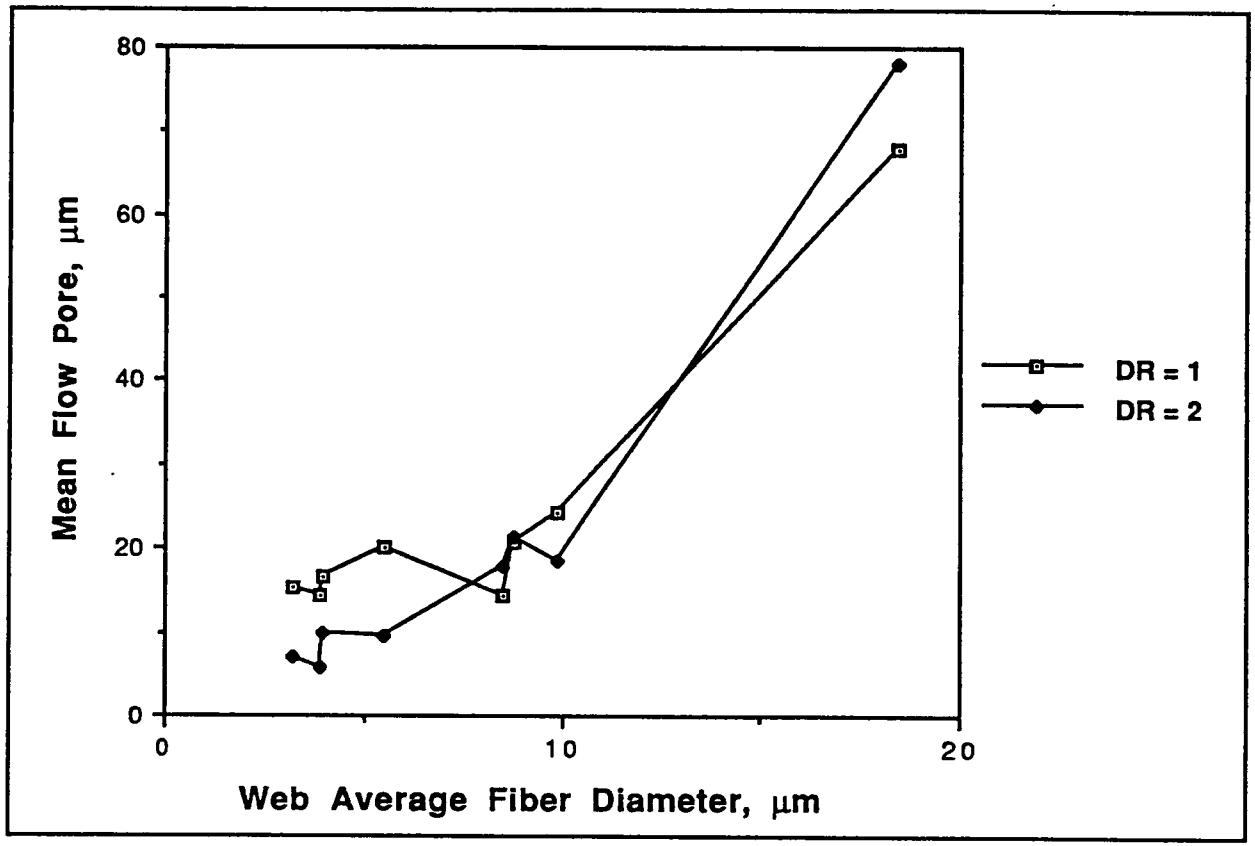


Figure 5.21 Plot of the mean flow pore size (MFP) for precursor webs and counterparts post processed to DR = 2.0 versus the average diameter of fibers in the web.

actually having large average diameter filaments. The fiber size distribution of the precursor webs is seen to be a limiting factor in the pore size consolidation achieved as illustrated in Figure 5.22 for packing density versus web average fiber diameter and Figure 5.23 for filtration efficiency versus web average fiber diameter. Each plot indicates an onset of improved filtration performance at fiber diameters less than ten micrometers. Euler buckling limitations associated with slenderness ratio to the third power requires that far greater compression is needed to transform the pore shape of webs having filaments of higher average filament diameters.

CONCLUSIONS

Precursor webs having a wide range of the maximum pore size, distribution and average fiber diameters were draw processed at different oven temperatures and draw ratio levels up to 2.5. Precursor webs of smaller average fiber diameter were processable to lower maximum pore size and filtration efficiency due to the slenderness ratio and rheological molecular orientation existing in the webs of finer fiber diameters. Drawing precursor webs that had average filament diameters less than about 10 micrometers was found to reduce the measures of pore size distribution up to one half that of the precursor. Post drawing produced particle collection efficiencies equivalent to that of undrawn webs having average fiber diameter up to one third smaller.

Changes in the maximum pore size due to web consolidation were

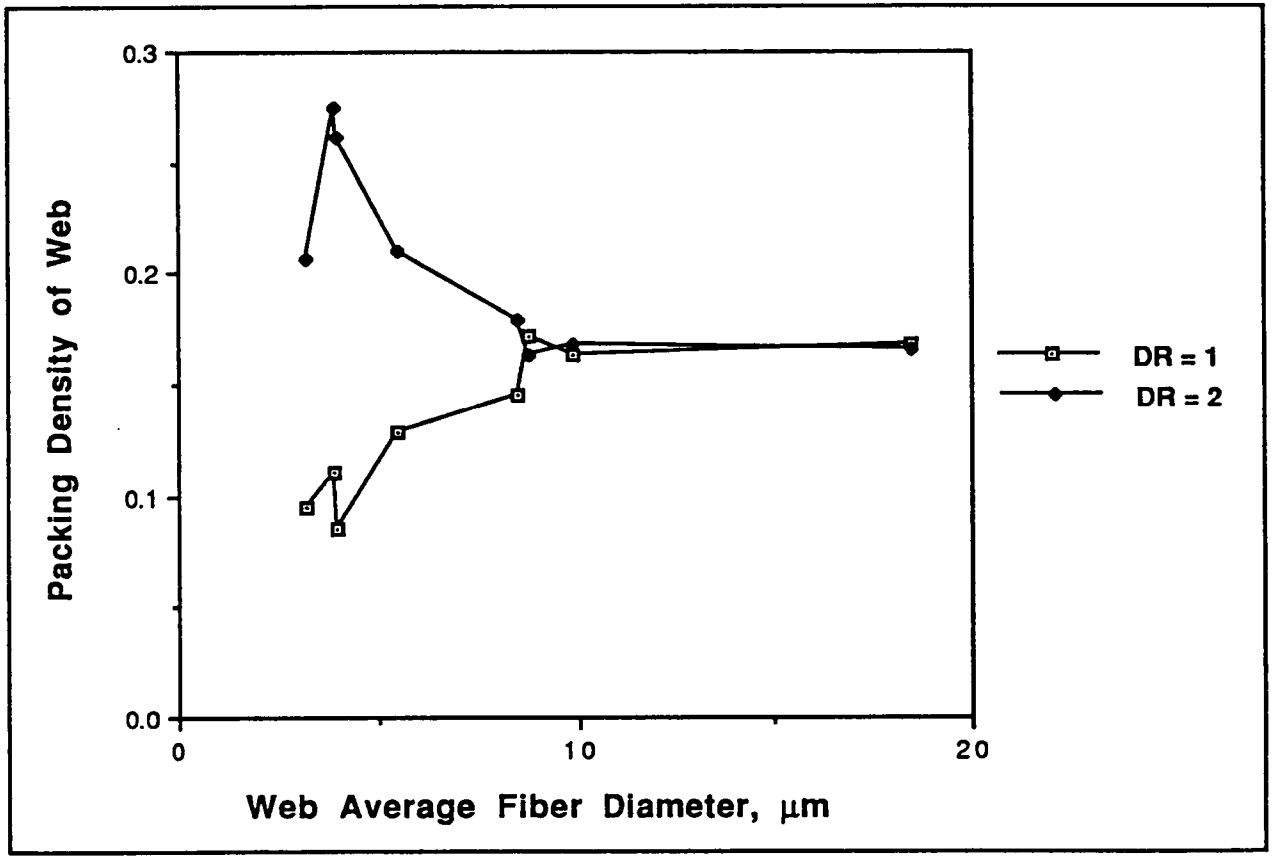


Figure 5.22 Plot of the packing density for precursor webs and counterparts post processed to DR = 2.0 versus the average diameter of fibers in the web.

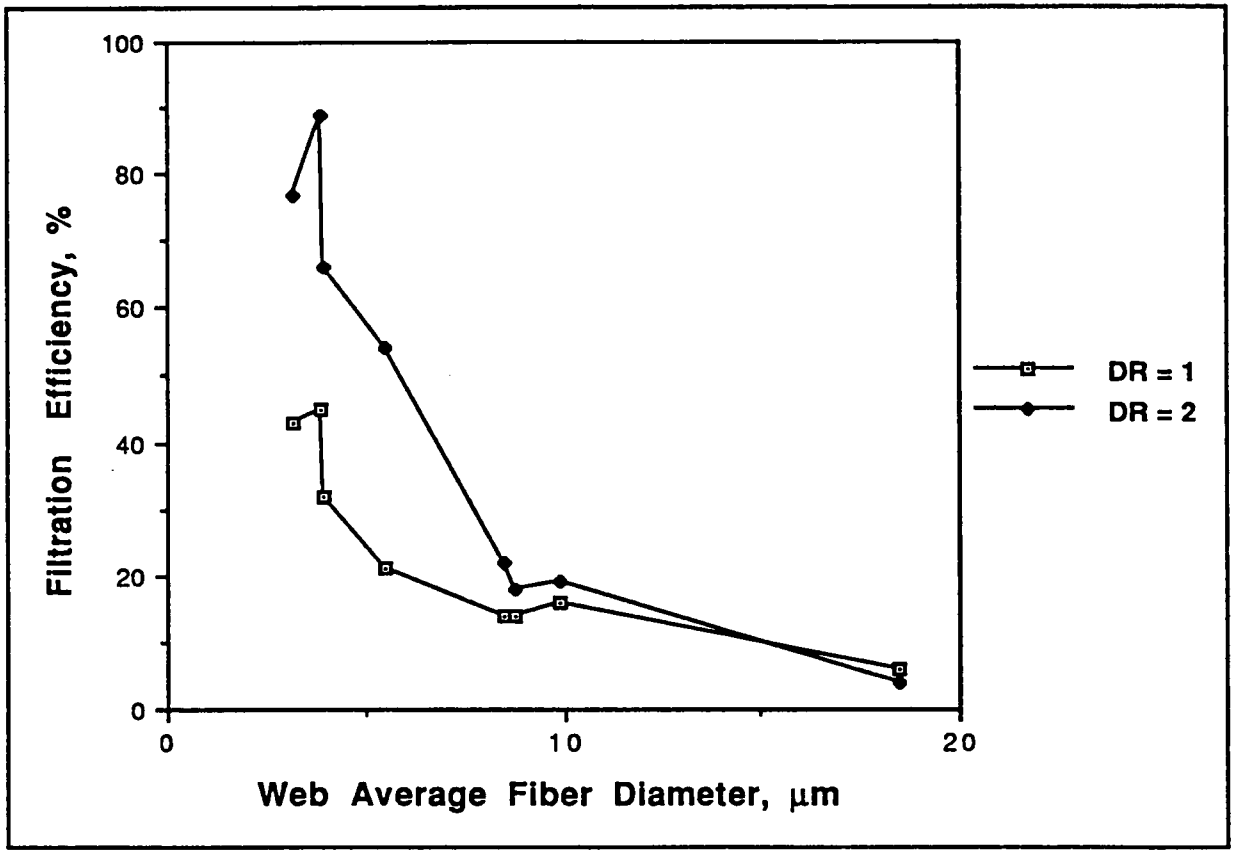


Figure 5.23 Plot of the particulate capture efficiency for precursor webs and counterparts post processed to DR = 2.0 versus the average diameter of fibers in the web.

collectively related to the ASTM 1289 particulate penetration (the compliment of filtration capture efficiency) and to Fraizer air permeability values of the drawn web. This implies that the filtration performance of the collection of meltblown webs processed at varied levels of hot drawing is predicted by the maximum pore size of the processed web. Further, new low levels of MPS can be achieved by post drawing precursor web having definable low levels of fiber diameter and initial pore size distribution. Subsequent calendering of these webs would further reduce the pore size distributions for enhanced filtration performance. The relative preservation of flow properties relative to calendering and the control of the pore size distribution establishes post drawn meltblown web product as a new filtration media for many new applications.

LIST OF REFERENCES

1. Cooper, Douglas W., Monitoring Contaminant Particles in Gases and Liquids: A Review, in Particles in Gases and Liquids - Detection, Characterization and Control, Mittal, K.L., Editor, 1987.

2. Davis, W.T., "Basic Fundamentals Affecting Pressure Drop and Efficiency", Report to TVA, 1971.

3. Cooper, C. David, and Alley, F.C., "Air Pollution Control: A Design Approach, PWS Engineering Boston, 1986.

4. Liu, B.Y.H., and Rubow, K.L., "Air filtration by Fibrous Media," Fluid Filtration: Gas, Volume I, ASTM STP 975, R. R. Raber, American Society For Testing and Materials, Philadelphia, 1986.

5. Ensor, D. S., et. al., "Particle Deposition Velocity in Silicon Technology", in Particles in Gases and Liquids - Detection, Characterization and Control, Mittal, K.L., Editor, 1987.

6. Wadsworth, L. C., and Goswami, B. C., "Nonwoven Fabrics: Spunbonded and Meltblown Processes", Proceedings of the Fiber Producer Conference, April 1983, Greenville, S.C., 1983.

7. Wente Van A., "Superfine Thermoplastic Fibers", Industrial and Engineering Chemistry, Vol. 48, No. 8, page 1342 - 1346, August 1956.

8. Hyun, S. Lim and Mayer, Ernest, "Tyvek For Microfiltration Media", Fluid/Particle Separation Journal, Vol.2, No.1, March, 1989.

9. Milligan, M. W. et. al., "The Use of Crossflow to Improve Nonwoven Melt-Blown Fibers", Journal of Applied Polymer Science, Vol. 44, 279-288, 1992.

10. Lee, Youngchul and Wadsworth, L. C., "Structure and Filtration Properties of Melt Blown Polypropylene Webs", Polymer Engineering and Science, Vol. 30, No. 22, November 1990.

11. Wadsworth, L. C. and Muschelewicz, A.O., "Effects of Resin And Process Variables on the Production of Ultrafine Melt Blown Polypropylene Fibers", Book of Papers, Fourth International Conference on Polypropylene Fibers and Textiles, East Midlands Conference Center, Nottingham, UK, September 23-25, 1987.

12. Gelmann Sciences Filter Book, Polypropylene Separators, page 36, 1991.

13. Wadsworth, L. C., Lee, Youngchul, and Barboza, Steven D., "Effects of

Melt Blown Web Structure on Filtration Efficiency and Porosity", Presentation at INDA-TEC 89 Conference Philadelphia, PA, June 1989.

14. Harding, John W. and Keller, James P., "Post-Drawn Melt-Blown Webs, U.S. Patent 4,048,364, September 13, 1977.

15. Cheremisinoff, N. P., Ed., Liquid Filtration/Fabric Filter Book, Ann Arbor Science, Woburn Mass., 1983.

16. Yeh, H. C., "Aerosol Filtration by Fibrous Filters--Part I. Theoretical", J. Aerosol Sci. 5:191-204, 1973.

17. Krcma, Radko, Manual of Nonwovens, Textile Trade Press, Manchester, England, 1971.

18. Cole, F. W., "Filter Ratings - An Alternative to Black Arts", Filtration and Separation 12 (1) p. 17 - 22, 1975.

19. DeBruyne, Roger, "The Use of the Coulter Porometer for the Characterization of Filter Media, Particularly Sintered Metal Fibre Bekipor Media", Hot Melt Polymer Filtration Conference, American Filtration Society, Clemson, SC, October 13-14, 1988.

20. Orr, Clyde,Filtration Principles and Practices, Part II, Marcel Dekker, Inc New York and Basel, 1979.

21. Buntin, R. R. and Lohkamp, D. T., TAPPI Vol.56, No.4, 74-77, 1973.

22. Petterson, S. R., "On the Mechanics of Nonwoven "Fabrics", ScD. thesis, Massachusetts Institute of Technology, 1958

23. Floden, John G., "Autogenously Bonded Composite Web", U.S. Patent #3,837,995, September 24, 1974.

24. Schwartz, Eckert, "Meltblowing Die for Strong Webs", U.S. Patent # 4,lookup, 1977.

25. Crangle, A. A., Laverty, J. J. and Ruddell, J. N., "M-Draw: A Novel Technique For Heat Transfer To Polymeric Materials", Book of Papers, Polypropylene Fibers and Textiles IV,

26. Weinkauf, D. H. and Paul, D. R., "Effects of Structural Order on Barrier Properties", in Barrier Polymers and Structures, Koros, William J., Ed.AACS Symposium Series, 0097-6156; 423, 1990

27. Ericson, C.W. and Baxter, J.F., "Spunbonded Nonwoven Fabric Studies I: Characterization of Filament Arrangement in the Web," Text. Res. J., 43, 371, 1973.

28. Orr, Clyde, Filtration: Principles and Practices, PartI, Marcel Dekker, Inc. New York and Basel, p110, 1979.

29. Lee, K.W., and Liu, B.Y.H., "Experimental Study of Aerosol Filtration by Fibrous Filters," Aerosol Sci. Technol. 1:35-46, 1982.

30. Lee, K.W., and Liu, B.Y.H., "Theoretical Study of Aerosol Filtration by Fibrous Filters," Aerosol Sci. Technol. 1:147-162, 1982.

31. Orr, Clyde, Filtration: Principles and Practices, PartI, Marcel Dekker, Inc. New York and Basel, p 154, 1979.

32. Orr, Clyde, Filtration: Principles and Practices, PartI, Marcel Dekker, Inc. New York and Basel, p 31, 1979.

33. Stippes, M., Wempner, G. and Beckett, R., The Mechanics of Deformable Bodies, Prentice-Hall International, Inc., London 1961.

34. Choi, K. J. et. al., Polymer Engineering and Science, Vol. 28, No.2, 81-89, 1988.

35. Samuels, Robert J., Structured Polymer Properties, John Wyley & Sons, New York, 1973.

VITA

Charles Bernard Hassenboehler, Jr. is a native of New Orleans, Louisiana and received a Bachelor of Science in Physics from the University of New Orleans in 1964. He worked in Fiber Physics and New Products at the United States Department of Agriculture in New Orleans where he developed innovations involving the mechanical behavior of materials and textile structures, and aerodynamics. He has over thirty publications and patents in varied areas of textile process, product, and test development. His studies and work at the University of Tennessee, Knoxville have centered on nonwoven and polymer processes with emphasis on meltblowing and spunbonding process innovations and products for filtration, medical and consumer applications. His pension for experimentation extends into his hobbies of fishing, boat racing and domestic innovations.